Neuron

Dissociable neuronal substrates of visual feature attention and working memory

Highlights

- Most cortical neurons show WM or attention signals, and not both
- LPFC-p inactivation during attention, but not during WM, impairs task performance
- Inactivation reduces neuronal attentional effects but minimally affects WM signals
- Feature attention and WM thus have dissociable neuronal substrates

Authors

Diego Mendoza-Halliday, Haoran Xu, Frederico A.C. Azevedo, Robert Desimone

Correspondence

diegomendoza@pitt.edu

In brief

Mendoza-Halliday and colleagues show that in multiple cortical areas, neurons modulated by visual feature attention are largely different from those encoding working memories. By optogenetically inactivating LPFC-p during attention or working memory, they further show that it plays a critical role in attentional modulation, but not in working memory.

Mendoza-Halliday et al., 2024, Neuron *112*, 850–863
March 6, 2024
https://doi.org/10.1016/j.neuron.2023.12.007

CellPress

CellPress
OPEN ACCESS

Neuron

Article

Dissociable neuronal substrates of visual feature attention and working memory

Diego Mendoza-Halliday,[1,2,*] Haoran Xu,[1] Frederico A.C. Azevedo,[1] and Robert Desimone[1]
[1]Department of Brain and Cognitive Sciences, McGovern Institute for Brain Research, Massachusetts Institute of Technology, Cambridge, MA, USA
[2]Lead contact
*Correspondence: diegomendoza@pitt.edu
https://doi.org/10.1016/j.neuron.2023.12.007

SUMMARY

Attention and working memory (WM) are distinct cognitive functions, yet given their close interactions, it is often assumed that they share the same neuronal mechanisms. We show that in macaques performing a WM-guided feature attention task, the activity of most neurons in areas middle temporal (MT), medial superior temporal (MST), lateral intraparietal (LIP), and posterior lateral prefrontal cortex (LPFC-p) displays attentional modulation or WM coding and not both. One area thought to play a role in both functions is LPFC-p. To test this, we optogenetically inactivated LPFC-p bilaterally during different task periods. Attention period inactivation reduced attentional modulation in LPFC-p, MST, and LIP neurons and impaired task performance. In contrast, WM period inactivation did not affect attentional modulation or performance and minimally affected WM coding. Our results suggest that feature attention and WM have dissociable neuronal substrates and that LPFC-p plays a critical role in feature attention, but not in WM.

INTRODUCTION

Top-down visual attention and working memory (WM) are among the most studied cognitive functions and the most affected by neurological and psychiatric disorders. Visual WM allows us to temporarily store representations of stimuli when they become visually unavailable. Visual attention allows us to select, among all visually available stimuli, those that are behaviorally relevant and enhance their processing. Thus, whereas visual attention is most essential when relevant stimuli are visually present, visual WM is most essential when the stimuli held in memory are visually absent.

Human studies using functional magnetic resonance imaging (fMRI) and electroencephalography (EEG) have reported a large overlap between the brain regions showing activity related to WM and attention, commonly including the lateral prefrontal cortex (LPFC) and parietal cortex.[1,2] This anatomical overlap has led many researchers to propose that WM and attention share the same underlying neuronal mechanisms[3] and that they are two constructs representing the same function.[2] However, one limitation of fMRI and EEG studies is that signals reflect the aggregate activity of millions of neurons. Single-neuron electrophysiological studies in non-human primates have mostly examined either whether the activity of neurons selectively encodes visual features maintained in WM[4–8] or whether neurons' visual responses are modulated by attention to these features.[9–13] Little is known about whether the same or different neurons participate in these two mechanisms.

Another argument used to claim that attention and WM share the same mechanisms is that they are strongly interdependent functions. Attention is thought to act as a gatekeeper for WM: attended stimuli are better encoded in WM.[3] In turn, it is believed that WM plays a key role in attention: attending to a visual stimulus feature is thought to require maintaining a WM representation of the target feature to be attended; this representation would serve as an attentional template signal that, through top-down mechanisms, selectively modulates the activity of feature-tuned visual cortical neurons. One area that has been proposed as a main source of top-down feature attentional signals is LPFC.[14–16] Neurons in the posterior end of LPFC (LPFC-p), including the ventral prearcuate (VPA) region, are modulated by attention to visual features.[17,18] Muscimol inactivation of VPA reduces feature attentional effects in the frontal eye field (FEF) and area V4 and causes behavioral deficits associated with feature attention.[18,19] It has also been shown that neurons in LPFC-p encode visual features maintained in WM.[20,21]

The above findings raised several important questions, which we aimed to address in this study. First, we investigated whether WM and attention signals are present in the same or different neurons in LPFC-p and other areas. We trained monkeys to perform a WM-guided spatially global feature attention task for motion direction. We recorded spiking activity from motion-direction-selective neurons in multiple cortical areas at different processing stages: middle temporal (MT), an early visual area; medial superior temporal (MST), a visual association area; lateral intraparietal (LIP); and LPFC-p. Second, we examined whether

LPFC-p plays a critical role in both feature attention and WM maintenance: we optogenetically inactivated it bilaterally during the task periods of WM maintenance or sustained attention and measured the effects on task performance and on the strength of WM and feature attention signals in neurons from the recorded areas.

RESULTS

We trained two rhesus macaque monkeys (*Macaca mulatta*) in a WM-guided feature attention task (Figure 1A). In each trial, a full-screen random dot surface with coherent motion in one of two opposite directions (cue stimulus) was presented for 0.8 s. After a 3.2-s delay period during which the monkeys maintained the cue direction in WM, we presented a test stimulus—two overlapping full-screen random dot surfaces moving in opposite directions, one in the cued direction. The monkeys were trained to selectively attend to the surface with the cued direction (i.e., target) to detect and report (releasing a hand-held lever) the occurrence of a small patch of dots with higher speed in the target surface while ignoring any patch in the other surface (i.e., distractor). Because the patch locations were randomly chosen across the screen (Figure S1), the monkeys were required to attend to all spatial locations. To our knowledge, this is the first attention task in non-human primates using spatially global stimuli and requiring feature attention to be allocated evenly across all spatial locations, therefore minimizing the recruitment of spatial attention.

We implanted 5 laminar probes acutely in each experimental session to simultaneously record the spiking activity of motion-direction-selective neurons from five cortical areas across various processing stages: MT (938 neurons), MST (1,865 neurons), LIP (570 neurons), and bilateral LPFC-p (1,271 neurons)—including posterior portions of areas 8Ad/v, 9/46d/v, and 45 (Figures 1B and 1C).[22] Because we simultaneously recorded multiple tens of neurons from various areas, neurons were expected to vary widely in their receptive field locations and sizes; the spatially global visual stimuli ensured that most neurons were visually stimulated and engaged in the task independently of their receptive field location or size.

Strength of WM coding and feature attentional modulation across the visual processing stream

We first examined whether the delay period spiking activity of each neuron encoded the cue direction held in WM and whether its response to the test stimulus was modulated by the attended cue direction (Figure 2A). We also estimated each neuron's sensory selectivity for motion direction during the cue presentation period. Importantly, because there was no stimulus present during the delay period other than the fixation point, differences in firing rates between the cue direction conditions were indicative of selectivity for memorized directions. Similarly, conditions with opposite cue directions had identical test stimuli, i.e., the same two overlapping moving surfaces with opposite directions (Figure 1A); thus, differences in test responses between these conditions were due to cue-direction-dependent attentional modulation. We computed the area under the ROC curve (auROC, rectified to above 0.5) to estimate the discriminability between the distributions of firing rates in trials with opposite cue directions during the cue period (sensory discriminability), delay period (WM discriminability) and test period before the target or distractor speed changes (attentional discriminability); these three discriminability values served as a measure of the strength of the sensory coding of motion direction, WM coding, and feature attentional modulation, respectively. The presence of discriminability was determined by the auROC's statistical significance (see STAR Methods).

We first examined how sensory coding, WM coding, and attentional modulation evolve across the visual processing stream. The percentage of neurons with significant sensory discriminability and the mean sensory discriminability across all neurons were the highest in the early visual cortex (MT) and followed a decreasing trend downstream (Figures 2B–2D). In contrast, the percentage of neurons with significant WM discriminability, as well as the mean WM discriminability, was remarkably low in the early visual cortex and increased progressively downstream (Figures 2B–2D). Similarly, for attention, the percentage of significant neurons and mean discriminability also increased in a downstream progression (Figures 2B–2D). These results, as were all subsequent results, were similar for both monkeys (Figure S2). The remaining figures show the results obtained from the combined neuronal populations of both monkeys.

Neuron-level dissociation between WM coding and attentional modulation

Next, we examined whether WM coding and feature attentional modulation are present in the same or different neurons and whether the co-occurrence of these two signals within neurons differs across processing stages. If WM and attention share the same neuronal substrates, then neurons that encode the memorized directions would be expected to be modulated by attention to these directions. In all areas, neurons showed a wide variety of combinations of WM discriminability and attentional discriminability. To determine the presence of WM and attentional signals in each neuron, we classified neurons in each area into three groups—"WM & attention" (Figure 2A, top), "WM-only" (Figure 2A, middle), and "attention-only" (Figure 2A, bottom)—based on the significance of WM and attentional discriminabilities (Figure 2E). Interestingly, the majority of neurons were WM-only and attention-only, and only a minority were WM & attention (Figures 2D–2F; Table S1). The proportion of WM & attention neurons was significantly lower than those of WM-only and attention-only neurons in all areas except LIP (Figure 2F; chi-squared tests for proportions, Bonferroni corrected). The proportion of WM & attention neurons differed significantly across areas and was by far the highest in LIP (Figure 2F; chi-squared tests for proportions, Bonferroni corrected). Notably, in most WM & attention neurons, motion direction preference was the same during the delay and test periods (Figures 2A top and S3). Among MT neurons, there was robust attentional discriminability but only rare and weak WM discriminability (Figures 2B and 2C). In the remaining areas, where there was a substantial fraction of both WM-only and attention-only neurons, we used multivariate population decoding (see STAR Methods) to confirm that in these subpopulations, WM and attention

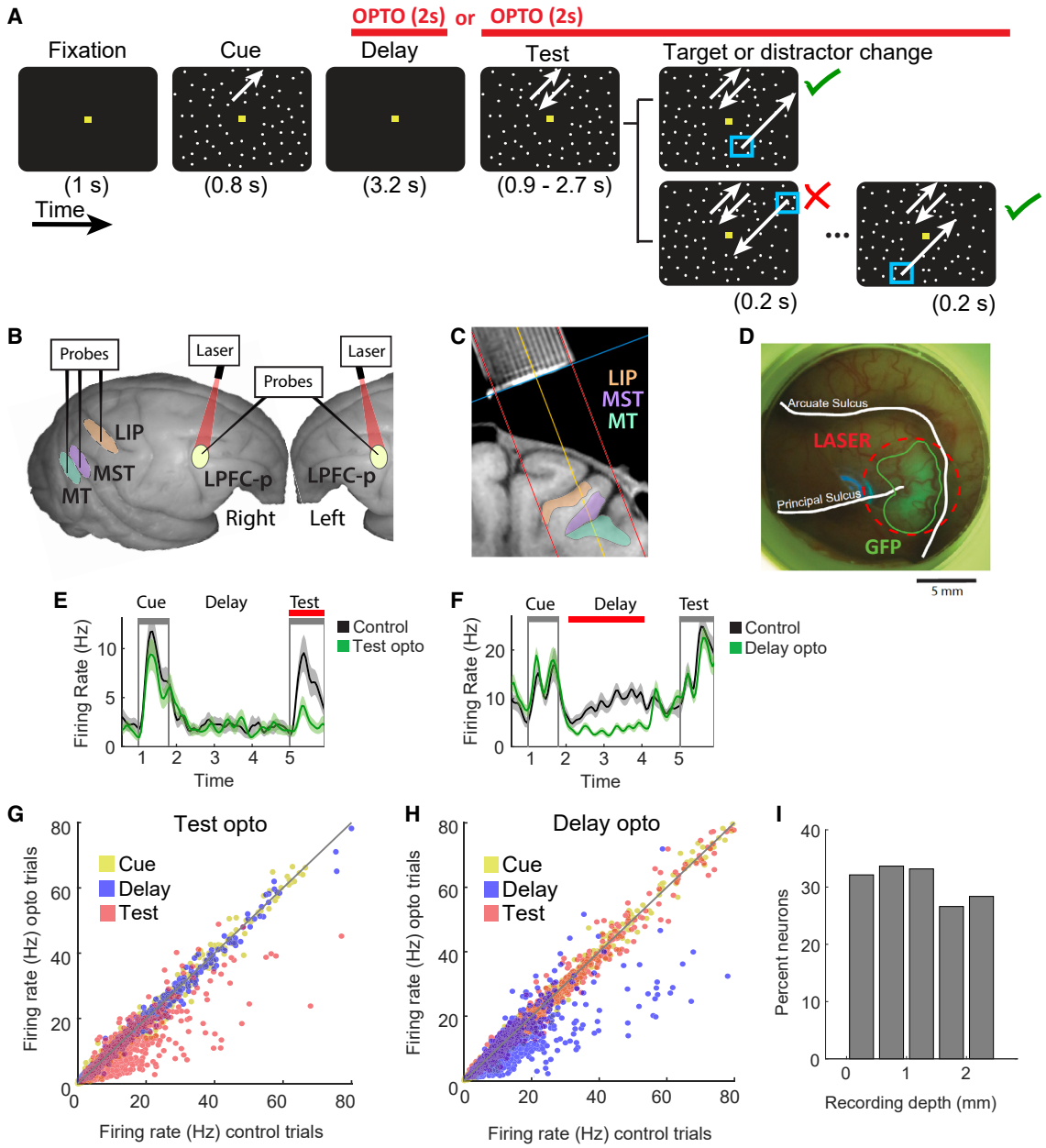

Figure 1. Behavioral, electrophysiological, and optogenetic methods

(A) Temporal sequence of behavioral task. Arrows depict the motion directions of dot surfaces; fixation point is yellow; cyan squares depict speed-changing dot patches; red segments show periods of optogenetic LPFC-p inactivation; and check mark and cross depict correct and incorrect responses, respectively.

(B) Macaque brain photograph showing approximate location of recorded and optogenetically stimulated areas. MT, MST, and LIP cortical areas are embedded within sulci.

(C) Structural MRI nearly coronal section of one monkey showing the recording chamber grid (top) and location of LIP, MST, and MT (right hemisphere) cortical areas. Red lines, range of available probe trajectories.

(D) Photograph of an example LPFC chamber from one monkey—taken using a blue light source (reflected on the dura) and yellow filter—showing cortical surface through a transparent artificial dura. GFP epifluorescence indicates viral expression region (enclosed by a green line). Dashed red line shows the area of laser illumination; white lines show sulci. Scale bar is shown below.

(E and F) Mean firing rate (± SEM) of two example neurons over time across trials with (green) and without (black) optogenetic stimulation in the test (E) or delay (F) period.

(G and H) Mean firing rate in cue, delay, and test periods across control trials (horizontal axis) and optogenetic inactivation (opto) trials (vertical axis) for all LPFC-p neurons recorded in test-opto sessions (G) and delay-opto sessions (H).

(I) Percent neurons with significant optogenetic modulation of firing rates recorded at various cortical depths.

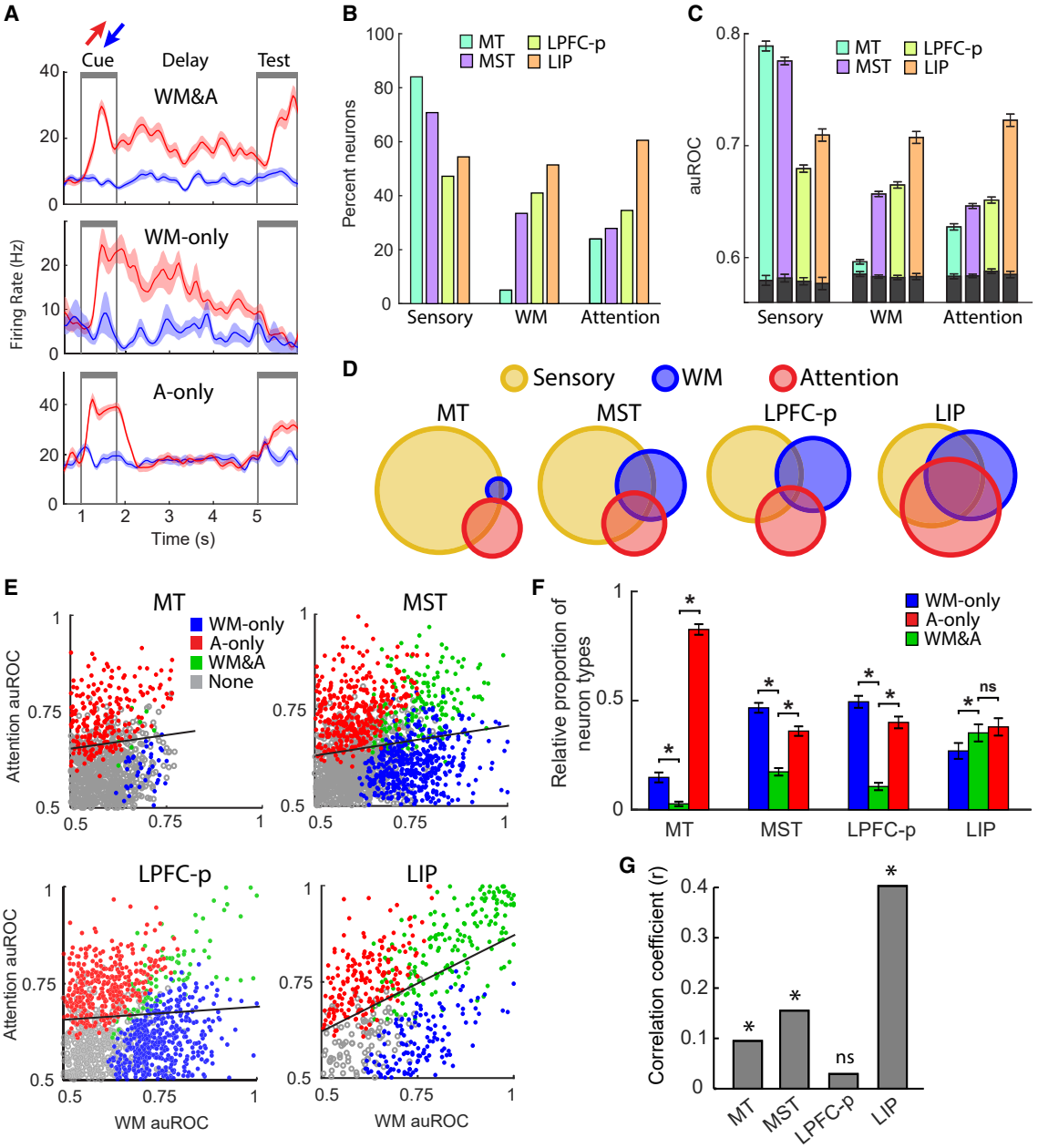

Figure 2. WM coding and feature attentional modulation of neuronal firing rates

(A) Mean firing rate (±SEM) over time across trials with opposite cue directions for examples of three functional types of neurons: working memory and attention (WM and A; LIP neuron), WM-only (LIP neuron), and A-only (MST neuron). Red/blue traces, preferred/anti-preferred directions (different for each neuron).

(B) Percent neurons with significant sensory, WM, and attentional discriminability in each brain area.

(C) Mean (±SEM) sensory, WM, and attentional discriminability (auROC) across neurons in each area. Gray bars indicate mean auROC (±SEM) expected by chance.

(D) Venn diagrams showing the relative proportion of neurons with significant sensory, WM, and/or attentional discriminability.

(E) WM and attentional discriminabilities (auROC) of all neurons (dots) color coded by the significance of WM and attentional discriminabilities. Black line, linear regression.

(F) Relative proportions of WM-only, WM and A, and A-only neuron types. *significant difference; ns, non-significant. Error bars, 95% confidence intervals for proportions.

(G) Spearman's coefficient (r) from the correlation between WM auROC and attention auROC across neurons in each area. *significant correlation ($p < 0.05$); ns, non-significant.

See also Figure S4.

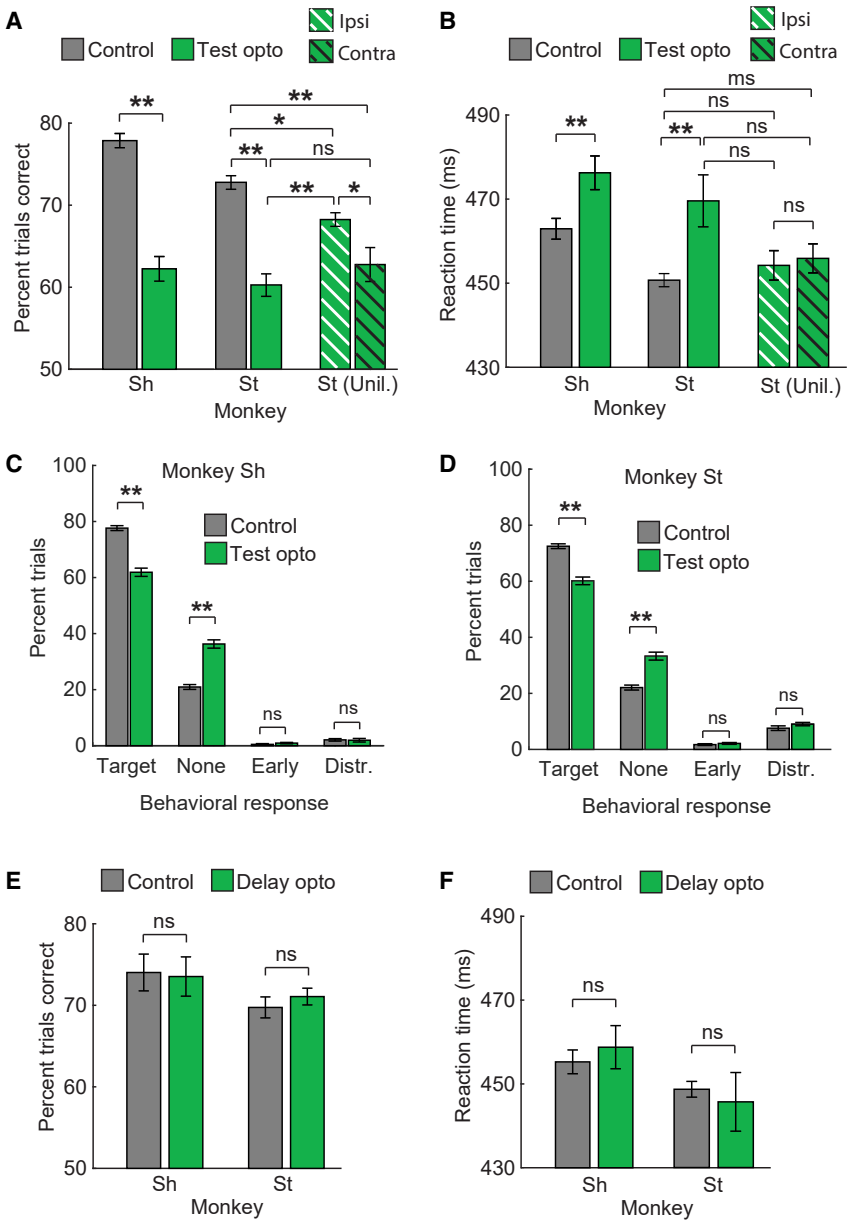

Figure 3. Behavioral effects of optogenetic prefrontal inactivation

(A and B) Mean (±SEM) task performance (A) and reaction time (B) across all test-opto sessions in the control (gray) and opto (green) conditions, for monkeys Sh and St. Striped bars: mean task performance (A) and reaction time (B) for monkey St in unilateral inactivation sessions in trials with target changes ipsilateral (white stripes) or contralateral (black stripes) to the inactivated hemisphere.

(C and D) Across-session mean (±SEM) percent trials with different behavioral response types for monkeys Sh (C) and St (D).

(E and F) Same as (A) and (B) for delay-opto sessions. *$p < 0.05$; **$p < 0.01$; ms, marginally significant ($p < 0.09$); ns, not significant.

signals were dissociable at the population coding level: for WM-only neurons, the population decoding of directions in WM was high, but the decoding of attended directions was near chance level (Figure S4A); for attention-only neurons, the population decoding was high for attended directions but near chance for directions in WM (Figure S4B). As expected, in the combined population of WM-only, attention-only, and WM & attention neurons, the decoding of directions in WM and attended directions were both high (Figure S4C).

Although we classified neurons by the significance of discriminability, neurons did not show any apparent clustering into discrete categories. To further examine the relationship between neurons' strength of WM and attentional signals along a continuum, we tested whether WM and attentional discriminabilities correlated across neurons. We found marked differences between areas (Figures 2E and 3G). In LPFC-p, there was no significant correlation (Spearman's correlation coefficient $r = 0.029$, $p = 0.30$). In both MT and MST, the correlation was significant but low (MT: $r = 0.095$, $p = 0.004$; MST: $r = 0.16$, $p < 0.001$). In contrast, the correlation in LIP was significant and much higher than that in other areas ($r = 0.40$, $p < 0.001$). These results are consistent with those obtained by classifying neurons into functional categories by the significance of WM and attentional discriminabilities (Figures 2E and 2F).

In sum, our results indicate that in LPFC-p and MST, WM and attention signals are present mostly in different neurons and that the magnitude of attentional modulation of individual neurons is unrelated or weakly related to their WM coding strength. In LIP, WM and attention signals co-occur in a higher percentage of neurons and are more strongly correlated. These findings suggest that the substrates of feature attention and WM are largely dissociated at the level of individual neurons in LPFC-p and MST, as well as in LIP to a lesser extent. This dissociation was present at the brain area level in MT, where attentional effects were present but WM coding was mostly absent.

Large-scale bilateral optogenetic inactivation of LPFC-p

It has been proposed that LPFC-p plays a role in WM maintenance and serves as a source of top-down feature attention signals to other cortical areas. The presence of LPFC-p neurons showing WM and/or attentional signals is compatible with this view but not sufficient to determine whether these neurons play a causal role in WM maintenance and feature attention. To test this, we developed a method for large-scale bilateral optogenetic LPFC-p inactivation during either the delay period (WM maintenance) or the test period (sustained feature attention). We

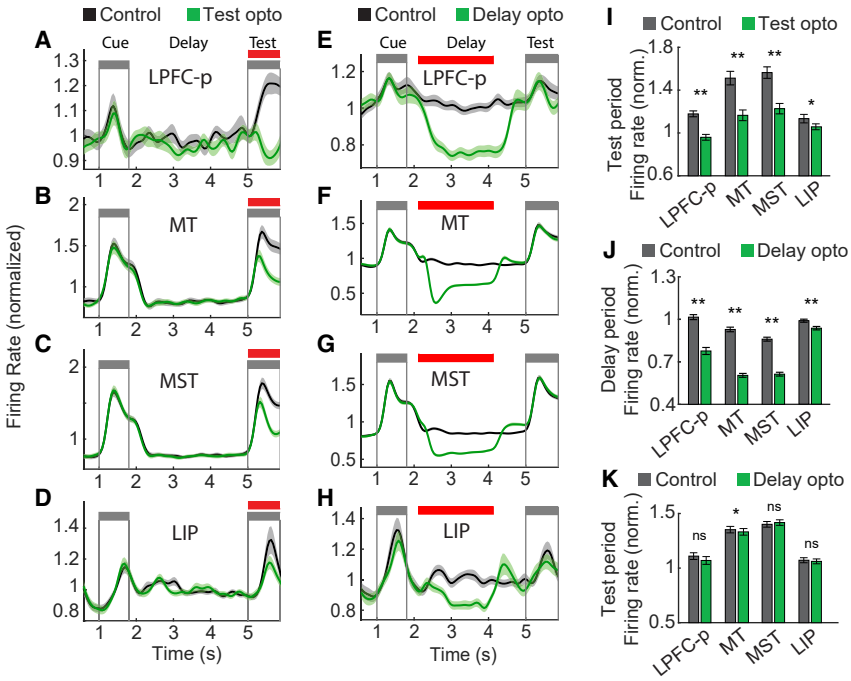

Figure 4. Effects of test and delay period optogenetic prefrontal inactivation on neuronal firing rates in each area

(A–H) Mean normalized firing rate (±SEM) over time in control and opto trials across neurons with significant optogenetic modulation in LPFC-p, MT, MST, and LIP during test-opto (A–D) and delay-opto (E–H) sessions. Red line, optogenetic stimulation period.

(I) Mean test period normalized firing rate (±SEM) in control and opto trials across neurons in (A)–(D).

(J and K) Mean delay period (J) and test period (K) normalized firing rate (±SEM) in control and opto trials across neurons in (E)–(H). *p < 0.05; *p < 0.01; ns, not significant.

See also Figure S5.

implanted transparent artificial duras in the two chambers covering left and right LPFC-p, adapting methods previously used by others.[23,24] The self-sealing property of the duras allowed us to perform approximately 170 injections of an AAV construct in 24 penetrations (12 per hemisphere) to drive the neuronal expression of the red-shifted inhibitory opsin Jaws[25,26] in a large area of left and right LPFC-p. Expression was confirmed *in vivo* by the visualization of GFP epifluorescence on the cortical surface through the artificial dura (Figure 1D) starting 2 weeks after injections and before each recording session. We estimated the mean cortical surface area showing expression to be approximately 50 mm^2 per hemisphere.

In each recording session, right and left LPFC-p were simultaneously inactivated via external illumination with red lasers placed 18–29 mm above the artificial duras. Our external illumination method ensured optical stimulation of the entire region of opsin expression in each hemisphere (Figure 1D). In some experimental sessions (“test-opto,” 22 in monkey Sh and 44 in monkey St), we optogenetically inactivated LPFC-p during the test period (starting at test onset and lasting 2 s or until the monkey’s response). In other sessions, (“delay-opto,” 30 in monkey Sh and 39 in monkey St), inactivation was performed for 2 s during the delay period (from 0.3 s after cue offset until 0.9 s before test onset). In both test-opto and delay-opto sessions, optical stimulation occurred randomly in half of the trials (i.e., opto trials), with the remaining trials serving as control (Figure 1A).

In each experimental session, a recording probe was lowered in each prefrontal chamber at a random location within the opsin expression region. We confirmed that optogenetic stimulation during the test or delay period decreased the firing rates of LPFC-p neurons specifically during the stimulated period, without extending into neighboring periods (Figures 1E–1H, 4A, 4E, S5A, and S5E). Across sessions, optogenetic modulation had a significant effect on firing rates in approximately one-third of the neurons. Firing rates were significantly reduced in 93.5% of those neurons and increased in 6.5% of those neurons. The percentage of modulated neurons was similar across recording depths, with a somewhat lower percentage at deeper recording locations (Figure 1I), likely due to decreases in the light penetration of the cortex.[25,27] Based on estimates of neuronal density,[28,29] the percentage of modulated neurons, and the mean surface area of the optically stimulated expression region in both hemispheres, we estimated that the mean total number of LPFC-p neurons with significant response modulation in each session was approximately 5.1 million.

The viral construct used the human synapsin (*hSyn*) promoter, known to drive opsin expression in both excitatory and inhibitory neurons.[30] Thus, expression was expected to occur non-specifically among these neuron types. Confirming this, we found that putative excitatory (broad-spiking) and putative inhibitory (narrow-spiking) neurons showed the same mean latency of optogenetic modulation (19 ms, see STAR Methods).

LPFC-p inactivation during sustained feature attention impaired task performance

We first investigated whether optogenetic LPFC-p inactivation during the sustained attention period (i.e., test period) impaired task performance. The percentage of correct trials was lower in test-opto trials than in control trials in 100% of the 22 recording sessions for monkey Sh and in 93% of the 44 sessions for monkey St. The mean percentage of correct trials across sessions was significantly lower in opto trials than in control trials for both monkeys (Figure 3A; one-tailed paired t tests, Sh: $p < 0.0001$, St: $p < 0.0001$). Moreover, the mean reaction time across sessions was significantly higher in opto trials than in control trials for both monkeys (Figure 3B; one-tailed Wilcoxon rank-sum tests, Sh: $p = 0.0044$, St: $p = 0.0018$). These results suggest that LFPC-p plays a causal role in feature attention.

To further examine the specificity of these behavioral impairments, we classified error trials into those with a response to

the distractor speed change, those with an early response (before the target change but not to the distractor change), or those with no response. If LPFC-p inactivation caused a specific deficit in selective feature attention, it should impair the detection of target speed changes (in the attended dot surface) but not distractor speed changes (in the unattended surface). Alternatively, if inactivation caused a non-selective perceptual deficit, it should impair the detection of both target and distractor changes. We tested these alternatives in monkey St, which made a considerable fraction of responses to the distractor speed changes (across-session mean = 8%; maximum = 28%). In contrast to the significant reduction in the percentage of target response (correct) trials caused by inactivation, the percentage of distractor response trials slightly increased with inactivation ($p = 0.08$; paired t test; Figure 3D). This suggests that the impairment in task performance was in fact due to a deficit of selective feature attention. For both monkeys, inactivation caused no significant change in the percentage of early error trials (Figures 3C and 3D; paired t tests, monkey Sh: $p = 0.16$; monkey St: $p = 0.34$). This suggests that the decrease in target responses with inactivation was not due to increased response impulsivity. Instead, this decrease was accounted for by a comparable significant increase in no-response error trials (Figures 3C and 3D; paired t tests, monkey Sh: $p < 0.0001$; monkey St: $p < 0.0001$), suggesting that inactivation caused the monkeys to more often fail to detect target speed changes.

Previous studies have suggested that LPFC shows hemispheric lateralization during attention, with each cerebral hemisphere playing a larger role when attention is allocated to the contralateral hemifield than to the ipsilateral hemifield.[18,31,32] To examine whether the behavioral effects of optogenetic LPFC-p inactivation reflect this lateralization, we carried out nine sessions in monkey St in which we inactivated LPFC-p unilaterally in the left or right hemisphere (rather than bilaterally) during the test period and compared task performance in trials in which the target speed change patch occurred in the visual hemifield ipsilateral or contralateral to the inactivated hemisphere. For example, a patch in the left hemifield during right hemisphere LPFC-p inactivation would belong to the contralateral condition. Consistent with the known functional lateralization, the mean performance across sessions was significantly lower in the contralateral condition than in the ipsilateral condition (Figure 3A, one-tailed paired t test, $p = 0.023$). The fact that the magnitude of the impairment in task performance is dependent on the relationship between the inactivated hemisphere and the visual hemifield of the target stimulus argues against other potential non-specific effects of optogenetic stimulation as a cause of the observed behavioral impairments. Furthermore, the mean performance across sessions in both unilateral inactivation conditions (ipsilateral and contralateral) was intermediate between the control and the bilateral inactivation conditions (Figure 3A). Thus, unilateral LPFC-p inactivation is sufficient to impair task performance, but the impairment is more severe with bilateral inactivation than with unilateral inactivation. Similarly, mean reaction times across sessions in the two unilateral inactivation conditions were intermediate between the control and bilateral inactivation conditions, although differences between conditions were only marginally significant or non-significant (one-tailed Wilcoxon rank-sum tests; see Figure 3B). Despite significantly lower task performance in the contralateral condition than in the ipsilateral condition, the mean reaction time was not significantly higher in the contralateral condition than in the ipsilateral condition (Figure 3B, one-tailed Wilcoxon rank-sum test, $p = 0.37$).

LPFC-p inactivation during the WM delay did not impair task performance

Next, we examined whether bilateral LPFC-p inactivation during the delay period impaired task performance. For both monkeys, there was no significant decrease in the mean percentage of correct trials (Figure 3E; one-tailed paired t tests, Sh: $p = 0.33$, St: $p = 0.88$) nor a significant increase in the mean reaction time (Figure 3F; one-tailed paired t tests, Sh: $p = 0.26$, St: $p = 0.68$) across sessions in the opto condition with respect to the control condition. In sum, bilateral optogenetic inactivation of LPFC-p during the test period leads to robust deficits in task performance, whereas the same inactivation during the delay period does not. This suggests that LPFC-p plays a critical role in feature attention but not in WM maintenance and that these two functions have dissociable mechanisms in LPFC-p.

Based on these results, we reasoned that optogenetic LPFC-p stimulation during the test period would cause alterations in neuronal activity that would impair task performance. Furthermore, given the known feedback projections from LPFC-p to visual and parietal areas that likely play a role in the task, including MT, MST, and LIP cortical areas, we hypothesized that LPFC-p inactivation would lead to changes in neuronal activity in these distant cortical areas; in contrast, we predicted that optogenetic LPFC-p stimulation during the delay period would alter activity in a manner that minimally affects task performance.

Test period LPFC-p inactivation decreased attentional modulation of neuronal responses

We investigated the effects of LPFC-p inactivation on the spiking activity of neurons in all the recorded areas. First, we compared the mean firing rates of neurons in each area across all opto trials vs. control trials. As expected, optogenetic stimulation during the test period drastically decreased the firing rates of neurons in LPFC-p (Figures 4A and 4I; paired t test; Figure S5A). Interestingly, test period stimulation also led to a significant reduction in the firing rate of neurons in MT, MST, and LIP cortical areas (to a lesser extent)—regions located far from the optogenetically stimulated region (Figures 4B–4D and 4I; paired t tests; Figures S5B–S5D). Thus, changes in LPFC-p activity have modulatory effects on the activity of visual and parietal neurons, probably via feedback connections.[7,33]

Next, we examined whether test period optogenetic LPFC-p inactivation reduced feature attentional modulation strength in LPFC-p and other recorded areas (Figure 5A) by comparing each neuron's attentional discriminability in control and opto trials. We first examined this among all neurons with optogenetically modulated firing rates (see STAR Methods), since these neurons were the most likely candidates to show changes in attentional effects with optogenetic inactivation. Among these neurons, inactivation significantly decreased the strength of attentional effects in LPFC-p (Figures 5B and 5F) and MST

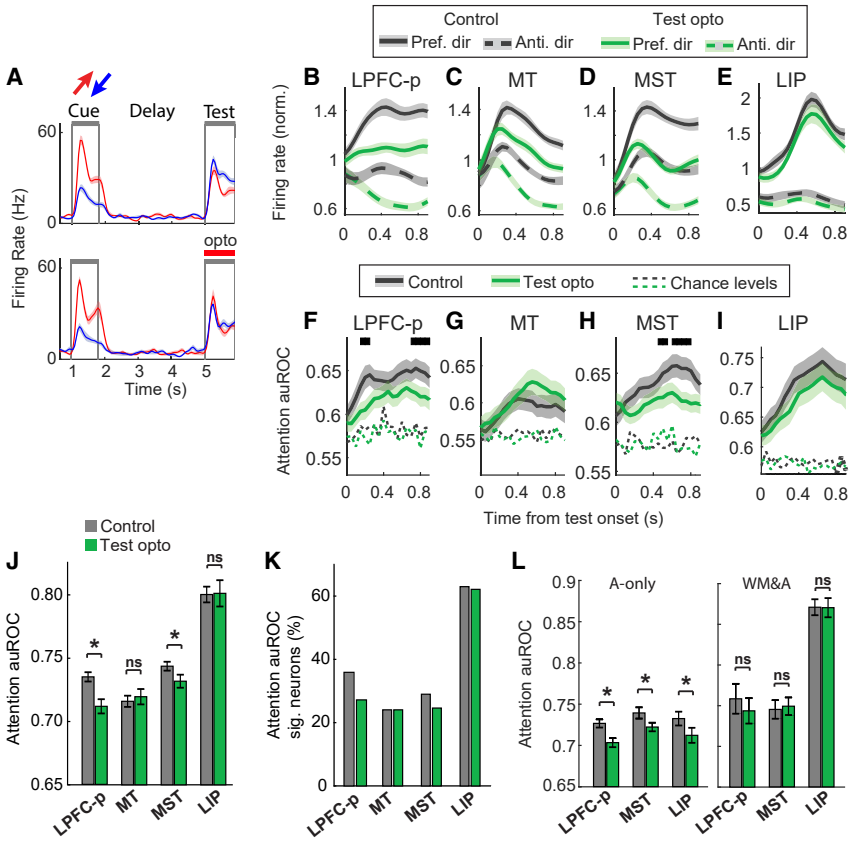

Figure 5. Effects of test period optogenetic prefrontal inactivation on attentional modulation

(A) Mean firing rate (±SEM) over time across trials with opposite cue directions (red and blue) for an example neuron (MST) with lower attentional discriminability in test-opto trials (bottom) than in control trials (top). Red segment, optogenetic stimulation period.

(B–E) Mean normalized firing rate (±SEM) during the test period across neurons in each area with significant optogenetic firing rate modulation in control and test-opto trials with preferred and anti-preferred attended directions.

(F–I) Mean auROC (±SEM) during the test period across neurons in (B)–(E) in control (gray) and test-opto (green) trials. Black segments, time bins with significant auROC difference between control and opto trials; dotted lines, mean auROC expected by chance in control and opto trials.

(J) For each area, mean attention auROC (±SEM) across neurons with significant attentional discriminability in control or test-opto trials.

(K) Percentage of neurons in each area with significant attentional discriminability in control or test-opto trials.

(L) Mean attention auROC (±SEM) across attention-only (left) and WM & attention (right) neurons in each area in control and test-opto trials. *$p < 0.05$; ns, not significant.

(Figures 5D and 5H; Wilcoxon rank-sum tests; see STAR Methods). To further quantify the magnitude of this effect at the individual neuron level, we computed for each neuron an auROC modulation index by measuring the percent change in attentional discriminability between control and opto conditions over time (see STAR Methods). Consistent with the above results, the distribution of modulation indices across neurons was shifted toward the negative range in LPFC-p and MST (Figures S6A and S6C). Thus, for the majority of LPFC-p and MST neurons, attentional discriminability decreased with LPFC-p inactivation.

We then reasoned that if the deficit in behavioral performance from test period LPFC-p inactivation (Figures 3A–3D) was due to a decrease in the strength of neuronal attentional effects, this decrease should be observable when averaged across the overall population of attention-related neurons, including neurons with and without significant optogenetic modulation of firing rates (see STAR Methods). In both LPFC-p and MST, a lower percentage of neurons showed significant attentional modulation in the test-opto condition than in the control condition (Figure 5K), and the mean attentional discriminability was significantly lower across neurons with attentional modulation in the test-opto condition than across neurons with attentional modulation in the control condition (Figure 5J; Wilcoxon rank-sum tests). Although prefrontal inactivation caused an overall decrease in firing rates in MT and LIP neurons (Figures 4B, 4D, 5C, and 5E), it did not significantly reduce the mean attentional effect across neurons with optogenetically modulated firing rates (Figures 5G, 5I, S6B, and S6D; Wilcoxon rank-sum tests; see STAR Methods) nor across all neurons with significant attentional effects (Figures 5J and 5K; Wilcoxon rank-sum tests; see STAR Methods).

As reported above, among neurons with significant attentional effects, some showed significant WM coding (WM & attention neurons), whereas others did not (attention-only neurons). We investigated whether attentional modulation strength was affected differently by LPFC-p inactivation in WM & attention vs. attention-only neurons. This comparison was possible in LPFC-p, MST, and LIP, where WM coding was prevalent in the neuronal population. In all three areas, test period inactivation led to a significant reduction in mean attentional discriminability among attention-only neurons but not among WM & attention neurons (Figure 5L; Wilcoxon rank-sum tests; see STAR Methods). Therefore, LPFC-p inactivation reduced the strength of attentional signals in these three areas, but only in neurons with no WM coding. The observation that LPFC-p inactivation reduced attentional effects not only locally but also distantly (in MST and LIP) supports the idea that LPFC-p serves as a source of feature attentional feedback signals that modulate neuronal responses in cortical areas along the visual processing stream. The reduction of attentional effects with test period LPFC-p inactivation may explain the observed impairments in task performance.

Effects of delay period LPFC-p inactivation on firing rates and WM coding

The lack of behavioral effects from delay period optogenetic LPFC-p inactivation suggested that there was a fundamental difference in the neuronal effects of delay vs. test period optogenetic stimulation. We first examined whether delay period optogenetic stimulation had an overall effect on firing rates. Stimulation significantly decreased firing rates not only in LPFC-p but also distantly in MT, MST, and LIP cortical areas (Figures 4E–4H and 4J; paired t tests, all $p < 0.01$; Figures S5E–S5H). Importantly, these firing rate decreases did not persist beyond the period of optogenetic stimulation: they were absent during the post-stimulation interval of the delay period (Figure S5I) and the test period (Figure 4K). Therefore, the lack of effects of delay period optogenetic stimulation on task performance cannot be due to a failure of our optogenetic methods to reduce delay period neuronal activity in LPFC-p and other recorded areas.

We then examined whether optogenetic LPFC-p inactivation during the delay period affected neuronal coding of the cue direction in WM, as measured by WM discriminability. We investigated this in LPFC-p, MST, and LIP, where there was prevalent WM discriminability. We first examined this among all neurons with optogenetically modulated firing rates (see STAR Methods), since these neurons were the most likely candidates to show changes in WM discriminability with optogenetic inactivation. Among these neurons in MST, delay period optogenetic stimulation caused a significant reduction in WM discriminability (Figures 6A, 6C, and 6F; Wilcoxon rank-sum tests). Confirming this, a lower percentage of MST neurons showed significant WM discriminability in the delay-opto condition than in the control condition (Figure 6I), and the mean WM auROC across neurons with significant WM discriminability in the delay-opto condition was significantly lower than that across neurons with significant WM discriminability in the control condition, even when pooling neurons with and without an optogenetic effect on overall firing rates (Figure 6H). However, the optogenetic effect on WM discriminability in MST was only temporary: it was not visible soon after the offset of optogenetic stimulation (Figures 6F and S5I). In LPFC-p and LIP, despite optogenetic stimulation causing an overall reduction in delay period firing rates (Figures 4E and 4H), this reduction was similar across cue direction conditions and did not lead to a significant reduction in WM discriminability (Figures 6B, 6D, 6E, 6G, 6H, and 6I; Wilcoxon rank-sum tests; see STAR Methods). Consistent with the above results, the distribution of WM auROC modulation indices across neurons was shifted toward the negative range in MST, but not in LPFC-p or LIP (Figures S6E–S6G; see STAR Methods). The absence of inactivation effects on WM coding in LPFC-p and LIP was further confirmed using a multivariate classification method to decode the memorized directions from population firing rate patterns (Figure S6J). In sum, LPFC-p inactivation led to a temporary reduction in the strength of WM coding in MST. In contrast, in LPFC-p and LIP, WM coding was robust to, and unaffected by, optogenetic modulations of firing rates.

We then asked whether in areas with considerable WM and attentional signals (LPFC-p, LIP, and MST), LPFC-p inactivation had different effects on WM & attention neurons and WM-only neurons. In MST, inactivation during the delay period significantly decreased the mean WM discriminability among WM-only neurons but not WM & attention neurons (Figure 6J; Wilcoxon rank-sum tests). Thus, the effect of prefrontal inactivation on WM coding was limited to MST neurons that exclusively carry WM signals but not attentional signals. In LPFC-p and LIP, there was no significant effect on WM discriminability for any of these neuron types (Figure 6J; Wilcoxon rank-sum tests).

Delay period LPFC-p inactivation did not reduce attentional modulation

The observation that prefrontal inactivation during the test period but not the delay period decreased task performance suggests that test period inactivation affects neuronal activity that is critical to the feature attention task, whereas delay period inactivation does not. It appeared that the critical activity for the task is the one modulated by attention during the test presentation, which allows the preferential processing of target speed changes. We therefore examined whether delay period prefrontal inactivation modulates test period neuronal activity and the strength of attentional modulation. Delay period optogenetic stimulation did not modulate overall firing rates during the test period in any recorded area (Figures 4E–4H and 4K; paired t tests, $p \geq 0.05$; a significant but very small 1.5% firing rate reduction was observed in MT) and did not significantly decrease the strength of attentional effects (Figure 6K; Wilcoxon rank-sum tests) or the percentage of neurons with significant attentional effects (Figure 6L) in any area. The fact that prefrontal inactivation during the test period, but not during the delay period, decreased both task performance and attentional effect strength in LPFC-p, MST, and LIP neurons suggests that the deficit in task performance was the result of decreases in attentional modulation. Finally, the observation that in LPFC-p, test period inactivation decreased attentional modulation (Figure 5J) but delay period inactivation did not affect WM coding (Figure 6H) or attentional modulation (Figure 6K) further supports the idea that the mechanisms of feature attention and WM are dissociated in this area. Noteworthy, this dissociation of effects was also present when limiting the analysis to LPFC-p neurons with a cue response or neurons with delay activity (Figures S6H and S6I; see STAR Methods), indicating that the dissociation is unaffected by these response properties.

DISCUSSION

In this study, we tested whether the neuronal substrates underlying feature attention and WM are dissociable. In all recorded areas, we found neurons with delay period activity encoding the directions maintained in WM and neurons with a response to the attended test stimuli that was modulated by the attended direction. This is in agreement with several human fMRI and EEG studies that have reported an overlap between brain regions with WM-related and feature-attention-related activities.[1,2] However, the majority of neurons in all areas showed WM or attention signals, but not both. Our results strongly suggest that within each area, partially different populations of neurons contribute to the mechanisms of feature attention and WM. It is likely that the

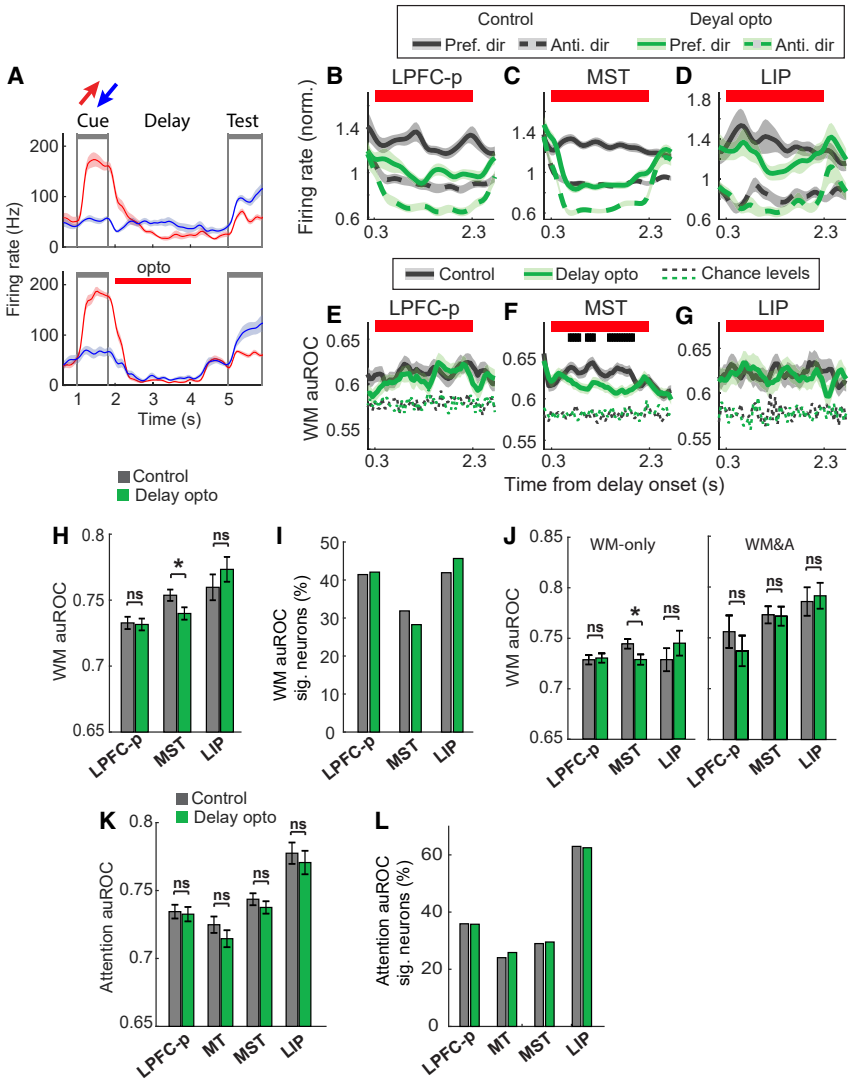

Figure 6. Effects of delay period optogenetic prefrontal inactivation on WM coding

(A) Mean firing rate (±SEM) over time across trials with opposite cue directions (red, blue) for an example neuron (MST) with lower WM discriminability in delay-opto trials (bottom) than in control trials (top). Red segment, optogenetic stimulation period.

(B–D) Mean normalized firing rate (±SEM) during the delay period across neurons in each brain area with significant optogenetic firing rate modulation in control and delay-opto trials with preferred and anti-preferred memorized directions.

(E–G) Mean auROC (±SEM) during the delay period across neurons in (B)–(D) in control and delay-opto trials. Black segments, time bins with significant auROC difference between control and opto trials; dotted lines, mean auROC expected by chance in control and opto trials.

(H) For each area, mean WM auROC (±SEM) across neurons with significant WM discriminability in control and delay-opto trials.

(I) Percent neurons in each area with significant WM discriminability in control and delay-opto trials. *p < 0.05; ns, not significant.

(J) Mean WM auROC (±SEM) across WM-only (left) and WM & attention (right) neurons in each area in control and delay-opto trials.

(K) For each brain area, mean attention auROC (±SEM) across neurons with significant attentional discriminability in control and delay-opto trials.

(L) Percentage of neurons in each brain area with significant attentional discriminability in control and delay-opto trials. *p < 0.05; ns, not significant.

single-neuron-level dissociation we report here was not detectable by human fMRI and EEG studies due to their low spatial resolution.[6] In agreement with previous studies, in early visual area MT, feature attention strongly modulated the activity of many neurons,[13] but WM signals were weak or absent[7,20]—an example of a region-level dissociation between the substrates of these two functions.

The observation that neurons showed a wide variety of combinations of WM discriminability and attention discriminability (WM-only, attention-only, and WM & attention) raises the question of whether the population contains mixed selectivity for features in WM and attended features. However, addressing this question requires an experimental design in which the feature in WM is independent of the attended feature. A previous study did examine the co-occurrence of WM and attention signals using such a design.[34,35] Similarly to our study, they found that attended locations and memorized locations were encoded mostly by different neurons. Importantly, among the minority of neurons that encoded both attended and memorized locations, some showed mixed selectivity,[36,37] i.e., nonlinear responses to combinations of memorized and attended locations. Mixed selectivity for WM and attention signals may allow these signals to be concurrently encoded[35,37] and used flexibly[38] and independently. This may allow the brain to concurrently maintain a visual feature/object in WM while attending to another[39] or to use a feature in WM to guide attention away from stimuli containing that feature.[40] However, the observation that WM & attention neurons were only a minority suggests that mixed selectivity does not represent a general principle across the entire population and that specialized neurons (WM-only and attention-only) without mixed selectivity are functionally essential.

To examine whether LPFC-p plays a causal role in feature attention and WM, we performed bilateral optogenetic LPFC-p inactivation. Although innumerable studies in mice and rats have successfully achieved robust behavioral effects by optogenetically perturbing neuronal activity in specific brain regions,[41] this has been achieved by a much lower fraction of macaque studies.[42] One potential reason is that given the much larger brain size in macaques than in mice and rats, the size of the perturbed regions using standard optogenetic approaches only represents a small fraction of typical functional regions in the macaque brain.[27] We implemented multiple improvements to

traditional approaches to inactivate a large surface area in LPFC-p. By implanting a self-sealing transparent artificial dura,[23,24] we achieved a large number of virus injections with anatomical precision, daily visualization of epifluorescence to track the extent of opsin expression over time, electrode penetrations for neuronal recordings without a guide tube (which typically destroys superficial cortical layers), and external laser stimulation of a large surface area matching the expression region. Although some studies have performed optogenetic stimulation through an artificial dura,[43,44] to our knowledge, none of them have achieved optogenetic inactivation of such a large cortical surface or bilateral inactivation of the same cortical area. Given the success of our study at achieving large-scale silencing of neuronal activity and robust behavioral effects, our methods provide a tool for future studies to silence large superficial cortical areas in macaques and other large species and generate observable behavioral effects.

We bilaterally inactivated LPFC-p during the test period to examine its role in feature attention. Test period inactivation strongly impaired task performance by selectively reducing the detection of speed changes in the attended target stimulus but not the unattended distractor stimulus. These results suggest that LPFC-p plays a causal role in selective feature attention. The lack of increases in distractor responses following inactivation is consistent with psychophysical studies showing that feature attention enhances the detection of attended features but not necessarily decreases the detection of unattended features.[45] An alternative interpretation is based on the notion that LPFC-p could play two roles in feature attention: first, it could participate in attentional selection—i.e., choosing which target feature to attend to and maintaining its representation (attentional template signal). If so, we would expect LPFC-p inactivation to impair the selection of the correct direction as a target, thus increasing distractor responses and decreasing target responses. Second, LPFC-p could play a role in the attentional modulation of visual cortex via feedback projections to enhance the processing of target features. If so, we would expect LPFC-p inactivation to impair the detection of target changes, decreasing target responses and increasing no-response trials. The observed decrease in target responses, an equivalent increase in no responses, and the absence of increases in distractor responses with inactivation suggest that LPFC-p plays a role in attentional modulation mechanisms but not in attentional selection. The top-down modulatory role of LPFC-p is supported by the observed reduction in attentional effects in MST and LIP neurons with LFPC-p inactivation (discussed below); however, the lack of its role in attentional selection remains largely speculative.

Interestingly, a recent study showed that in LPFC and other areas, there is an overlap between the neuronal population code underlying the attentional selection of a visual target among two stimuli and the code underlying the selection of a WM representation among two stored representations.[46] Thus, although our study suggests a dissociation between the mechanisms of attentional modulation and WM coding in LPFC-p, this study suggests an overlap between the mechanisms underlying attentional selection and the selection among WM representations in LPFC. The idea that LPFC may play a role in the attentional selection of target stimuli among distractors is supported by another study showing that in a selective attention task, large unilateral LPFC lesions impair the orientation discrimination of targets in the presence of distractors, but not in their absence.[47] However, because recordings and lesions in the above studies included LPFC subregions other than LPFC-p, it may be that attentional selection mechanisms involve these other subregions.

We also found that LPFC-p inactivation reduced attentional effects on neuronal activity in LPFC-p, MST, and LIP, suggesting that LPFC-p plays a critical role as a source of top-down feature attentional signals that selectively modulate stimulus responses in visual and parietal cortical neurons. Similar behavioral and neuronal effects (in FEF and V4) have been observed following muscimol inactivation of the VPA region within LPFC-p.[18,19] Interestingly, the observation that LPFC-p inactivation reduced attentional effects in attention-only neurons but not in WM and attention neurons in MST and LIP cortical areas indicates that the top-down modulatory signals from LPFC-p preferentially target neurons that are not involved in WM coding. It also suggests that besides LFPC-p, there may be other sources of attentional signals projecting to WM and attention neurons in MST and LIP. Why we found no significant decrease in attentional effects in MT with LPFC-p inactivation remains unclear.

Surprisingly, our study found that WM coding was much stronger in LIP than in LPFC-p (Figures 2B and 2C), suggesting potentially a more important role of LIP than LPFC-p in the maintenance of visual feature representations in WM. Consistent with this, synchronous interactions between LIP and LPFC during WM mostly originate in LIP.[48] Also surprisingly, we found that feature attentional effects in LIP[49–51] were much stronger than those in LPFC-p (Figures 2B and 2C), suggesting that LIP may be a source of feature attentional signals in addition to LPFC-p.[52] Supporting this, the unilateral muscimol inactivation of LIP impairs visual search in the contralateral hemifield.[53] Furthermore, LPFC-p inactivation caused weaker firing rate decreases in LIP neurons than in MST and MT neurons, suggesting that the top-down modulation of LPFC-p on LIP is weaker than that on other visual areas and that LIP acts more as a source than a recipient of top-down attentional signals.[51] This notion may help explain why LPFC-p inactivation reduced, but did not completely impair, task performance and attentional effects in MST and LIP. Moreover, the proportion of neurons in which WM and attention signals overlapped and the correlation between the strength of these signals within neurons were much higher in LIP than in other areas, suggesting that LIP may play a stronger role in the transformation of WM signals into attentional modulatory signals than LPFC-p and other areas.

One of our most notable findings was that task performance was strongly impaired by test period LPFC-p inactivation but unaffected by delay period inactivation. Consistent with this, delay period inactivation did not reduce the strength of WM representations in LPFC-p or LIP, and it only did so in WM-only neurons in MST; this effect was confined to the inactivation period, indicating that WM representations were restored in MST after the offset of inactivation. In summary, LPFC-p inactivation during the test period reduced attentional modulation and impaired task performance, whereas inactivation during the WM period

did not affect attentional modulation or performance and minimally reduced WM coding. These results suggest that LPFC-p plays a critical role in attention, but not WM, and, therefore, that the mechanisms of feature attention and WM are dissociable in LFPC-p. Whether these functions are dissociable in other subregions of LPFC remains to be investigated.

The lack of behavioral effects of delay period LPFC-p inactivation suggests that the activity of LPFC-p neurons encoding WM representations observed in our study and others[4–8] may not be critical for WM storage. There are several possible reasons. First, neurons with WM coding have been found in regions of LPFC other than LPFC-p,[38,54] which may be more important for WM storage. Second, a related possibility suggested by lesion studies is that LPFC is not necessary for the mere storage of WM representations and that LPFC subregions anterior and dorsal to LPFC-p play a critical role when WM representations are actively monitored or manipulated.[55,56] A third proposed alternative that remains mostly theoretical is that LPFC-p contributes to WM storage, but it does so via a synaptic or other activity-silent mechanism—one that does not depend on spiking activity.[57,58] We also used multivariate decoding methods to test the effects of delay period inactivation on population measures of WM that did not depend on changes in neurons' sustained firing rates, but we also found no effects in LPFC-p. Finally, it has been suggested that WM representations are stored in a widely distributed network of brain regions and that no single region plays a critical role in WM storage.[59] Consistent with this, our study shows that WM representations of motion direction are simultaneously encoded by neurons in at least three areas—MST, LIP, and LPFC-p. In contrast, our findings suggest that the mechanisms that generate feature attentional modulation are less distributed and rely more critically on LPFC-p.

Dissociations between various neural and behavioral signatures of attention and WM have been reported by several studies using EEG,[60,61] fMRI,[62,63] and behavioral measures[64] in healthy subjects and subjects with attention-deficit/hyperactivity disorder (ADHD)[65] and fronto-parietal strokes.[66] Complementing these findings, our results indicate that feature attention and WM do not rely on the same neuronal substrates and are two distinct functions rather than two constructs representing the same function.

STAR★METHODS

Detailed methods are provided in the online version of this paper and include the following:

- KEY RESOURCES TABLE
- RESOURCE AVAILABILITY
  - Lead contact
  - Materials availability
  - Data and code availability
- EXPERIMENTAL MODEL AND STUDY PARTICIPANT DETAILS
- METHOD DETAILS
  - Behavioral task and performance
  - Behavioral data analyses
  - Surgical procedures
  - Electrophysiological recordings
  - Optogenetic stimulation
  - Electrophysiological data analysis

SUPPLEMENTAL INFORMATION

Supplemental information can be found online at https://doi.org/10.1016/j.neuron.2023.12.007.

ACKNOWLEDGMENTS

We thank Hang Le, Briana McRae, and Callie Kunz for assistance with spike sorting; R. Ono for assistance with the anatomical mapping of recorded brain regions; and A. Marino and T. Inbar for assistance with behavioral training, implant care, and probe implantation. This work was supported by NIH R01-EY029666.

AUTHOR CONTRIBUTIONS

Funding acquisition, R.D.; study design, D.M.-H. and R.D.; animal training and data collection and analysis, D.M.-H.; writing – original draft, D.M.-H.; writing – revised draft, D.M.-H., R.D., H.X., and F.A.C.A.; implant design, surgical implantation, and virus injections, D.M.-H. and H.X.; and probe insertion and implant care, D.M.-H. and F.A.C.A.

DECLARATION OF INTERESTS

R.D. is a member of the *Neuron* Advisory Board.

Received: May 12, 2023
Revised: October 10, 2023
Accepted: December 12, 2023
Published: January 15, 2024

REFERENCES

1. Jonikaitis, D., and Moore, T. (2019). The interdependence of attention, working memory and gaze control: behavior and neural circuitry. Curr. Opin. Psychol. *29*, 126–134.
2. Olivers, C.N.L. (2008). Interactions between visual working memory and visual attention. Front. Biosci. *13*, 1182–1191.
3. Awh, E., and Jonides, J. (2001). Overlapping mechanisms of attention and spatial working memory. Trends Cogn. Sci. *5*, 119–126.
4. Konecky, R.O., Smith, M.A., and Olson, C.R. (2017). Monkey prefrontal neurons during sternberg task performance: full contents of working memory or most recent item? J. Neurophysiol. *117*, 2269–2281.
5. Lara, A.H., and Wallis, J.D. (2014). Executive control processes underlying multi-item working memory. Nat. Neurosci. *17*, 876–883.
6. Leavitt, M.L., Mendoza-Halliday, D., and Martinez-Trujillo, J.C. (2017). Sustained activity encoding working memories: not fully distributed. Trends Neurosci. *40*, 328–346.
7. Mendoza-Halliday, D., Torres, S., and Martinez-Trujillo, J.C. (2014). Sharp emergence of feature-selective sustained activity along the dorsal visual pathway. Nat. Neurosci. *17*, 1255–1262.
8. Warden, M.R., and Miller, E.K. (2010). Task-dependent changes in short-term memory in the prefrontal cortex. J. Neurosci. *30*, 15801–15810.
9. Bichot, N.P., Rossi, A.F., and Desimone, R. (2005). Parallel and serial neural mechanisms for visual search in macaque area V4. Science *308*, 529–534.
10. Ibos, G., and Freedman, D.J. (2014). Dynamic integration of task-relevant visual features in posterior parietal cortex. Neuron *83*, 1468–1480.
11. Maunsell, J.H.R., and Treue, S. (2006). Feature-based attention in visual cortex. Trends Neurosci. *29*, 317–322.

12. McAdams, C.J., and Maunsell, J.H.R. (1999). Effects of attention on orientation-tuning functions of single neurons in macaque cortical area V4. J. Neurosci. *19*, 431–441.
13. Treue, S., and Martínez Trujillo, J.C. (1999). Feature-based attention influences motion processing gain in macaque visual cortex. Nature *6736*, 575–579.
14. Desimone, R., and Duncan, J. (1995). Neural mechanisms of selective visual attention. Annu. Rev. Neurosci. *18*, 193–222.
15. Gregoriou, G.G., Rossi, A.F., Ungerleider, L.G., and Desimone, R. (2014). Lesions of prefrontal cortex reduce attentional modulation of neuronal responses and synchrony in V4. Nat. Neurosci. *17*, 1003–1011.
16. Rossi, A.F., Pessoa, L., Desimone, R., and Ungerleider, L.G. (2009). The prefrontal cortex and the executive control of attention. Exp. Brain Res. *192*, 489–497.
17. Lennert, T., and Martinez-Trujillo, J. (2011). Strength of response suppression to distracter stimuli determines attentional-filtering performance in primate prefrontal neurons. Neuron *70*, 141–152.
18. Bichot, N.P., Heard, M.T., DeGennaro, E.M., and Desimone, R. (2015). A source for feature-based attention in the prefrontal cortex. Neuron *88*, 832–844.
19. Bichot, N.P., Xu, R., Ghadooshahy, A., Williams, M.L., and Desimone, R. (2019). The role of prefrontal cortex in the control of feature attention in area V4. Nat. Commun. *10*, 5727.
20. Zaksas, D., and Pasternak, T. (2006). Directional signals in the prefrontal cortex and in area MT during a working memory for visual motion task. J. Neurosci. *26*, 11726–11742.
21. Mendoza-Halliday, D., and Martinez-Trujillo, J.C. (2017). Neuronal population coding of perceived and memorized visual features in the lateral prefrontal cortex. Nat. Commun. *8*, 15471.
22. Paxinos, G., Huang, X.W., and Toga, A.W. (2000). The Rhesus Monkey Brain in Stereotaxic Coordinates (Academic Press).
23. Nandy, A.S., Nassi, J.J., and Reynolds, J.H. (2017). Laminar organization of attentional modulation in macaque visual area V4. Neuron *93*, 235–246.
24. Ruiz, O., Lustig, B.R., Nassi, J.J., Cetin, A., Reynolds, J.H., Albright, T.D., Callaway, E.M., Stoner, G.R., and Roe, A.W. (2013). Optogenetics through windows on the brain in the nonhuman primate. J. Neurophysiol. *110*, 1455–1467.
25. Acker, L., Pino, E.N., Boyden, E.S., and Desimone, R. (2016). FEF inactivation with improved optogenetic methods. Proc. Natl. Acad. Sci. USA *113*, E7297–E7306.
26. Chuong, A.S., Miri, M.L., Busskamp, V., Matthews, G.A.C., Acker, L.C., Sørensen, A.T., Young, A., Klapoetke, N.C., Henninger, M.A., Kodandaramaiah, S.B., et al. (2014). Noninvasive optical inhibition with a red-shifted microbial rhodopsin. Nat. Neurosci. *17*, 1123–1129.
27. Gong, X., Mendoza-Halliday, D., Ting, J.T., Kaiser, T., Sun, X., Bastos, A.M., Wimmer, R.D., Guo, B., Chen, Q., Zhou, Y., et al. (2020). An ultrasensitive step-function opsin for minimally invasive optogenetic stimulation in mice and macaques. Neuron *107*, 38–51.e8.
28. Collins, C.E., Airey, D.C., Young, N.A., Leitch, D.B., and Kaas, J.H. (2010). Neuron densities vary across and within cortical areas in primates. Proc. Natl. Acad. Sci. USA *107*, 15927–15932.
29. Young, N.A., Collins, C.E., and Kaas, J.H. (2013). Cell and neuron densities in the primary motor cortex of primates. Front. Neural Circuits *7*, 41681.
30. Diester, I., Kaufman, M.T., Mogri, M., Pashaie, R., Goo, W., Yizhar, O., Ramakrishnan, C., Deisseroth, K., and Shenoy, K.V. (2011). An optogenetic toolbox designed for primates. Nat. Neurosci. *14*, 387–397.
31. Buschman, T.J., and Miller, E.K. (2007). Top-down versus bottom-up control of attention in the prefrontal and posterior parietal cortices. Science *315*, 1860–1862.
32. Tremblay, S., Pieper, F., Sachs, A., and Martinez-Trujillo, J. (2015). Attentional filtering of visual information by neuronal ensembles in the primate lateral prefrontal cortex. Neuron *85*, 202–215.
33. Xu, R., Bichot, N.P., Takahashi, A., and Desimone, R. (2022). The cortical connectome of primate lateral prefrontal cortex. Neuron *110*, 312–327.e7.
34. Lebedev, M.A., Messinger, A., Kralik, J.D., and Wise, S.P. (2004). Representation of attended versus remembered locations in prefrontal cortex. PLoS Biol. *2*, e365.
35. Messinger, A., Lebedev, M.A., Kralik, J.D., and Wise, S.P. (2009). Multitasking of attention and memory functions in the primate prefrontal cortex. J. Neurosci. *29*, 5640–5653.
36. Rigotti, M., Barak, O., Warden, M.R., Wang, X.J., Daw, N.D., Miller, E.K., and Fusi, S. (2013). The importance of mixed selectivity in complex cognitive tasks. Nature *7451*, 585–590.
37. Fusi, S., Miller, E.K., and Rigotti, M. (2016). Why neurons mix: high dimensionality for higher cognition. Curr. Opin. Neurobiol. *37*, 66–74.
38. Parthasarathy, A., Herikstad, R., Bong, J.H., Medina, F.S., Libedinsky, C., and Yen, S.C. (2017). Mixed selectivity morphs population codes in prefrontal cortex. Nat. Neurosci. *20*, 1770–1779.
39. Mendoza, D., Schneiderman, M., Kaul, C., and Martinez-Trujillo, J. (2011). Combined effects of feature-based working memory and feature-based attention on the perception of visual motion direction. J. Vis. *11*, 11.
40. Woodman, G.F., and Luck, S.J. (2007). Do the contents of visual working memory automatically influence attentional selection during visual search? J. Exp. Psychol. Hum. Percept. Perform. *33*, 363–377.
41. Fenno, L., Yizhar, O., and Deisseroth, K. (2011). The development and application of optogenetics. Annu. Rev. Neurosci. *34*, 389–412.
42. Tremblay, S., Acker, L., Afraz, A., Albaugh, D.L., Amita, H., Andrei, A.R., Angelucci, A., Aschner, A., Balan, P.F., Basso, M.A., et al. (2020). An open resource for non-human primate optogenetics. Neuron *108*, 1075–1090.e6.
43. Nandy, A., Nassi, J.J., Jadi, M.P., and Reynolds, J. (2019). Optogenetically induced low-frequency correlations impair perception. eLife *8*, e35123.
44. Nassi, J.J., Avery, M.C., Cetin, A.H., Roe, A.W., and Reynolds, J.H. (2015). Optogenetic activation of normalization in alert macaque visual cortex. Neuron *86*, 1504–1517.
45. White, A.L., and Carrasco, M. (2011). Feature-based attention involuntarily and simultaneously improves visual performance across locations. J. Vis. *11*, 15.
46. Panichello, M.F., and Buschman, T.J. (2021). Shared mechanisms underlie the control of working memory and attention. Nature *7855*, 601–605.
47. Rossi, A.F., Bichot, N.P., Desimone, R., and Ungerleider, L.G. (2007). Top down attentional deficits in macaques with lesions of lateral prefrontal cortex. J. Neurosci. *27*, 11306–11314.
48. Salazar, R.F., Dotson, N.M., Bressler, S.L., and Gray, C.M. (2012). Content-specific fronto-parietal synchronization during visual working memory. Science *338*, 1097–1100.
49. Ibos, G., and Freedman, D.J. (2016). Interaction between spatial and feature attention in posterior parietal cortex. Neuron *91*, 931–943.
50. Levichkina, E., Saalmann, Y.B., and Vidyasagar, T.R. (2017). Coding of spatial attention priorities and object features in the macaque lateral intraparietal cortex. Physiol. Rep. *5*, 5.
51. Sapountzis, P., Paneri, S., and Gregoriou, G.G. (2018). Distinct roles of prefrontal and parietal areas in the encoding of attentional priority. Proc. Natl. Acad. Sci. USA *115*, E8755–E8764.
52. Kastner, S., and Ungerleider, L.G. (2000). Mechanisms of visual attention in the human cortex. Annu. Rev. Neurosci. *23*, 315–341.
53. Wardak, C., Olivier, E., and Duhamel, J.R. (2004). A Deficit in covert attention after parietal cortex inactivation in the monkey. Neuron *42*, 501–508.
54. Riley, M.R., Qi, X.L., and Constantinidis, C. (2017). Functional specialization of areas along the anterior–posterior axis of the primate prefrontal cortex. Cereb. Cortex *27*, 3683–3697.
55. Petrides, M. (1991). Monitoring of selections of visual stimuli and the primate frontal cortex. Proc. Biol. Sci. *246*, 293–298.

56. Petrides, M. (2005). Lateral prefrontal cortex: architectonic and functional organization. Philos. Trans. R. Soc. Lond. B Biol. Sci. *360*, 781–795.

57. Mongillo, G., Barak, O., and Tsodyks, M. (2008). Synaptic theory of working memory. Science *319*, 1543–1546.

58. Stokes, M.G. (2015). 'Activity-silent' working memory in prefrontal cortex: a dynamic coding framework. Trends Cogn. Sci. *19*, 394–405.

59. Christophel, T.B., Klink, P.C., Spitzer, B., Roelfsema, P.R., and Haynes, J.D. (2017). The distributed nature of working memory. Trends Cogn. Sci. *21*, 111–124.

60. Bae, G.Y., and Luck, S.J. (2018). Dissociable decoding of spatial attention and working memory from EEG oscillations and sustained potentials. J. Neurosci. *38*, 409–422.

61. Harris, A.M., Jacoby, O., Remington, R.W., Becker, S.I., and Mattingley, J.B. (2020). Behavioral and electrophysiological evidence for a dissociation between working memory capacity and feature-based attention. Cortex *129*, 158–174.

62. Mayer, J.S., Roebroeck, A., Maurer, K., and Linden, D.E.J. (2010). Specialization in the default mode: task-induced brain deactivations dissociate between visual working memory and attention. Hum. Brain Mapp. *31*, 126–139.

63. Tomasi, D., Chang, L., Caparelli, E.C., and Ernst, T. (2007). Different activation patterns for working memory load and visual attention load. Brain Res. *1132*, 158–165.

64. Tas, A.C., Luck, S.J., and Hollingworth, A. (2016). The relationship between visual attention and visual working memory encoding: A dissociation between covert and overt orienting. J. Exp. Psychol. Hum. Percept. Perform. *42*, 1121–1138.

65. Mattfeld, A.T., Whitfield-Gabrieli, S., Biederman, J., Spencer, T., Brown, A., Fried, R., and Gabrieli, J.D.E. (2016). Dissociation of working memory impairments and attention-deficit/hyperactivity disorder in the brain. NeuroImage Clin. *10*, 274–282.

66. Peers, P.V., Astle, D.E., Duncan, J., Murphy, F.C., Das Hampshire, A., T., and Manly, T. (2020). Dissociable effects of attention vs working memory training on cognitive performance and everyday functioning following fronto-parietal strokes. Neuropsychol. Rehabil. *30*, 1092–1114.

67. Mulliken, G.H., Bichot, N.P., Ghadooshahy, A., Sharma, J., Kornblith, S., Philcock, M., and Desimone, R. (2015). Custom-fit radiolucent cranial implants for neurophysiological recording and stimulation. J. Neurosci. Methods *241*, 146–154.

68. Yger, P., Spampinato, G.L.B., Esposito, E., Lefebvre, B., Deny, S., Gardella, C., Stimberg, M., Jetter, F., Zeck, G., Picaud, S., et al. (2018). A spike sorting toolbox for up to thousands of electrodes validated with ground truth recordings in vitro and in vivo. eLife *7*, e34518.

69. Cardillo, G. (2008). ROC Curve: Compute a Receiver Operating Characteristics Curve (Math-Works).

70. Meyers, E.M. (2013). The neural decoding toolbox. Front. Neuroinform. *7*, 47170.

71. Torres-Gomez, S., Blonde, J.D., Mendoza-Halliday, D., Kuebler, E., Everest, M., Wang, X.J., Inoue, W., Poulter, M.O., and Martinez-Trujillo, J. (2020). Changes in the proportion of inhibitory interneuron types from sensory to executive areas of the primate neocortex: implications for the origins of working memory representations. Cereb. Cortex *30*, 4544–4562.

STAR★METHODS

KEY RESOURCES TABLE

REAGENT or RESOURCE	SOURCE	IDENTIFIER
Bacterial and virus strains		
AAV5.hSyn.Jaws-KGC.GFP.ER2-WPRE.hG	Penn Vector Core	AV-5-PV3638
Deposited data		
Data	This study	https://doi.org/10.5061/dryad.547d7wmfr
Experimental models: Organisms/strains		
Macaca mulatta	Covance and Alpha Genesis	N/A
Software and algorithms		
Matlab	Mathworks Inc.	N/A
Analysis code	This study	https://doi.org/10.5061/dryad.547d7wmfr

RESOURCE AVAILABILITY

Lead contact

Further information and requests for resources should be directed to the lead contact, Diego Mendoza-Halliday (diegomendoza@pitt.edu).

Materials availability

This study did not generate new unique reagents.

Data and code availability

The data analyzed in this study, and analysis code, have been deposited in Dryad and are publicly available as of the date of publication. The DOI is listed in the key resources table.

Any additional information required to reanalyze the data reported in this paper is available from the lead contact upon request.

EXPERIMENTAL MODEL AND STUDY PARTICIPANT DETAILS

Two male Rhesus macaque monkeys (*macaca mulatta*) were used in this study. All procedures were approved by the MIT Committee on Animal Care and were in accordance with the guidelines of the National Institutes of Health Guide for the Care and Use of Laboratory Animals.

METHOD DETAILS

Behavioral task and performance

The behavioral task was run on a PC computer using Psychomonkey/Psychtoolbox in Matlab (MathWorks, USA). Visual stimuli were presented on an LCD monitor (61 x 34.3 cm) with 120 Hz refresh rate (Acer, Taiwan). During task performance, each subject sat on a plexiglass chair at a viewing distance of 57cm, and the head was held with a headpost. Eye position was tracked using a camera-based Eyelink 2 system with 500 Hz sampling rate.

To examine the mechanisms underlying feature attention and working memory (WM) within the same neurons, we designed a WM-guided feature attention task requiring subjects to maintain a visual feature in WM, and subsequently use that feature to guide attention. The subject fixated on a small yellow square (0.6-by-0.6 visual degrees) presented at the center of the screen during the entirety of each task trial (fixation window radius: 2.6 visual degrees). Eye movements away from this window terminated a trial without reward. The subject began each trial (Figure 1A) by grasping a lever. After a 1000 ms fixation period, a cue stimulus was presented for 800 ms, consisting of a full-screen surface of random dots with coherent motion (5 dots/deg^2; 0.15 deg dot diameter; 10.9deg/s dot speed, 667 ms dot life) in one of two possible directions (45° clockwise from upward or 45° clockwise from downward). Monkey Sh was further trained to perform the task with four possible cue directions separated by 90°. After a 3200 ms delay period containing the fixation point alone, two test stimuli were presented, consisting of two overlapping full-screen random-dot surfaces with the same parameters as the cue. One of them – the target surface – matched the cue motion direction, whereas the other – the distractor surface – had motion in the opposite direction. Subsequently, a squared patch of dots (length 8.14 degrees) at a randomly-selected

location within the target surface (Figure S1) increased motion speed (to double the original) for 250 ms and returned to its initial speed. The target speed change onset occurred at a random time between 900 and 2700 ms from test onset. In half of the trials, the speed-changing patch occurred in the distractor surface, followed by a second patch occurring in the target surface at a random time (minimum 800 ms after the distractor patch and maximum 2700 ms from test onset). The subject was required to selectively attend to the test surface matching the cue direction (i.e., the target) in order to detect the occurrence of the target speed change and report it by releasing the lever, while ignoring distractor changes. A correct trial occurred when the subject released the lever within a response window of 120 to 580 ms from target change onset. A 1 mL juice reward was then delivered to the subject with an automated juicer. The reaction time was measured as the time between target speed change onset and lever release. Lever releases during the test period (after 900 ms) but before the target speed change were classified as early response errors; releases within 120 to 580 ms from distractor onset were classified as distractor response errors. Trials with no lever release before the end of the response window were classified as no-response errors. Task performance was quantified as the percentage of correct trials over the sum of all correct and error trials defined above. Trials with either a lever release before the test or a fixation loss were excluded from the analyses.

We varied the perceptual difficulty of the task between trials by varying the percentage of speed-changing dots within the target/distractor patches (85%, easier; 55%, intermediate; or 35%, difficult). These trials were presented randomly and with equal frequency. Difficult trials imposed higher attentional demands to correctly perform the task, thus ensuring that monkeys selectively attended to the target surface throughout the session. We confirmed this by ensuring that performance in difficult trials was considerably higher than expected by chance in all sessions. However, only including difficult trials would risk subjects losing motivation to perform the task or eventually un-learning the task rule due to low performance. This was prevented by including easier trials. In a pilot test, naïve human subjects instructed to perform the task were generally unable to detect most speed changes until they had trained for several trials to selectively attend to the target while ignoring the distractor.

Behavioral data analyses

We used one-tailed paired t tests to test whether each monkey's mean task performance (percent correct trials) across all test-opto sessions was significantly lower in test-opto trials than control trials, and whether mean task performance (percent correct trials) across all delay-opto sessions was significantly lower in delay-opto trials than control trials. Paired t tests were also used to test for significant differences between test-opto and control conditions in each monkey's mean percentage of (1) distractor response trials, (2) early error trials, and (3) no-response error trials across test-opto sessions. Mean task performance across sessions was compared between the contralateral and ipsilateral conditions using a one-tailed paired t test. To test whether each monkey's mean reaction time across all test-opto sessions was significantly higher in test-opto trials than control trials and whether mean reaction time across all delay-opto sessions was significantly higher in delay-opto trials than control trials, we used one-tailed Wilcoxon Rank Sum Tests. We also used one-tailed Wilcoxon Rank Sum Tests to test whether mean reaction times across sessions in each of the two unilateral inactivation conditions was significantly higher than the control condition and significantly lower than the bilateral inactivation condition, and whether mean reaction time was significantly lower in the contralateral than the ipsilateral inactivation condition. Non-parametric tests were used to test differences in reaction times due to largely unequal variances between the compared conditions.

Surgical procedures

Head post and cranial chamber implantation

All surgical procedures were performed while animals were under anesthesia. Animals were provided analgesics and antibiotics after surgery. Each monkey was first surgically implanted with a titanium headpost over the posterior end of the skull. After recovery from surgery was complete, animals began task training while being head-fixed with a head-post holder. After the period of training was completed, a second surgery was performed for implantation of cranial chambers. We first performed round craniotomies over left and right prefrontal cortex, and left parietal cortex. We then performed a durotomy in each prefrontal cranial window and implanted a round transparent silicone artificial dura so that its edge was slid under the native dura around the perimeter of the durotomy. Subsequently, we implanted three cranial chambers over the three craniotomies. Each prefrontal chamber was designed so that its bottom edge was inserted into the craniotomy and touched the artificial dura (instead of sitting on the skull surface like standard implants). The transparent artificial dura windows allowed for multiple optogenetic and electrophysiological procedures including virus injections, continuous *in vivo* visual tracking of viral expression, minimally-invasive external optical stimulation, and electrophysiological recordings.

Chambers were made of polyether ether ketone (PEEK) and had an inner diameter of 19 mm. Using structural magnetic resonance imaging (MRI) of the skull and brain, each chamber was custom-designed with a base to fit the surrounding skull,[67] and was attached to it with ceramic screws. The headpost implanted in the first surgery was similarly custom-fit to the skull and attached to it with titanium screws. All custom-fit implants were fabricated with a 5-axis CNC machine. The parietal chamber implant had a cylinder protruding over the base, onto which the electrophysiological recording towers were mounted. Prefrontal chamber implants were designed without a protruding cylinder; instead, the cylinder was screwed and affixed to the base before recording sessions. The three chambers were placed over the left and right prefrontal cortex, and left parietal cortex. Prefrontal chambers were positioned to include the region between the arcuate sulcus and the posterior segment of the principal sulcus. The parietal chamber was placed and oriented for probe trajectories to access areas LIP, MST, and MT as perpendicularly as possible to the cortical sheet (Figure 1C).

Chambers were cleaned 3 to 5 times per week under aseptic conditions. The prefrontal chambers were rinsed using a sterile saline antibiotic cocktail with 2.5% Penicillin G Sodium powder (USP 5 million units) and 5% Amikacin (0.25 g/mL). After rinsing, a gauze piece was placed on the artificial dura with a drop of a second saline cocktail (16% Penicillin and 40% Amikacin); a silicone disc was then placed over the gauze to maintain moderate pressure on the dura, and a water-tight cap was placed and screwed on top of the chamber. The parietal chamber was rinsed using sterile saline and betadine solution. During chamber cleaning, we also monitored the health of the prefrontal cortical tissue, as well as the progression of native dura regrowth. When enough dura had regrown to occlude visibility of the cortical surface, we repeated the durotomy procedure following all surgical standards described above. This was only necessary after 6 months from the initial durotomy, and only once for each monkey during the period of experimental sessions.

A structural MRI scan was performed after the implantation surgery to obtain an anatomical map of the chamber locations. Each chamber's recording grid (see Electrophysiological recordingssection) was filled with a 1% agar solution in sterile water with 0.8% Ablavar (gadolinium-based contrast agent) and placed inside the chamber for the duration of the scan. The MR images served to map the position of the chamber and grid, and the transcortical probe trajectories corresponding to all grid slots (Figure 1C).

Virus injections

To induce neuronal expression of the opsin Jaws in left and right LPFC-p, we performed injections of the AAV5.hSyn.Jaws-KGC.GFP.ER2-WPRE.hG viral construct (Penn Vector Core). The following setup was prepared identically for each prefrontal hemisphere. Injections were made with a 9.6 cm long 31 GA needle. The needle was reinforced by inserting it and gluing it to an 8.3 cm-long 23 GA needle, keeping 8mm of the tip exposed for injection penetration. The reinforcement needle was held by a microdrive tower (NAN Instruments, Israel) on an XY table fixed to the chamber. The needle was attached to a 70-cm Intramedic polyelthylene tubing, which was in turn attached to a 25-μL Hamilton syringe mounted on a syringe pump (Harvard Apparatus, USA). These attachments were sealed with Bondic glue and made air-tight.

Virus injections were performed two to three weeks after chamber implantation, under the same surgical conditions described above. The left and right prefrontal chambers were first cleaned. Then, the towers with injection needles were mounted on the chambers. In each hemisphere, we selected twelve injection locations in a grid-like layout distributed across the LPFC-p subregion between the arcuate sulcus and the posterior end of the principal sulcus. Neighboring injection locations were approximately 1.6 mm apart. Locations were shifted away from any visible blood vessel. Injections were performed serially at each of the twelve locations, beginning with the most central location and spiraling outwards along the grid of planned locations. The needle was quickly shifted between injection locations using the microdrive tower's XY table. At each location, we lowered the needle to penetrate the artificial dura and cortex, and we stopped at a depth of 4 mm below where the needle had dimpled the dura. We performed the first injection at that depth (1 μL), and subsequent injections by retracting the needle in steps of 1 mm until 2 mm deep (1 μL), and then in steps of 0.5 mm (0.5 μL) until the needle was out of the cortex.

The above surgical implantation and injection procedures were developed and tested on a pilot monkey prior to performing them on the two trained monkeys. This allowed the materials and procedures to be optimized. In one prefrontal chamber of the pilot monkey, we injected three different versions of the Jaws viral construct: one with AAV5, and two with AAV8, from different vector cores/batches. Visual inspection of GFP epifluorescence through the artificial dura helped determine that the AAV5 construct led to the most widespread expression. This construct was selected for the experiments.

Electrophysiological recordings

We recorded intracortical neuronal signals using V-Probes and S-Probes (Plexon Inc., USA) – multi-contact linear electrophysiological probes (i.e., laminar probes). Probes were 110 to 130 mm long and had 16 or 32 contacts (i.e., channels) with 150 or 100 μm spacing, respectively. Each probe was mounted on an electric microdrive tower (NAN Instruments, Israel) attached to the chamber, and was embedded in a guide tube (costume-cut spinal needle; sharp for parietal probes, blunt for prefrontal probes). The probe and guide tube were moved independently of each other by an electric microdrive and by hand, respectively. In preparation for a recording session, we mounted one probe on each prefrontal chamber and three on the parietal chamber. A plastic grid was placed in the parietal chamber, and the guide tube with the probe was placed inside a grid slot. Using the structural MRI images, the grid slot coordinates of the probe and its planned final depth were selected to target the cortical location of interest (Figure 1C).

After mounting all microdrive towers on the chambers, we manually lowered all guide tubes to poke through the native dura (for parietal chamber recordings) or to press and dimple the artificial dura (for prefrontal chamber recordings). The probes were then slowly inserted into the cortex using the computer-controlled electric microdrive, stopping at the planned final depth. The exact target depth was adjusted based on the presence of single- and multi-unit spiking activity across a large range of recording channels. In each session, we recorded activity from four to five probes simultaneously – one per prefrontal chamber and three in the parietal chamber. The three parietal chamber probes were placed to target areas LIP, MST and MT. Electrophysiological signals were recorded using a Blackrock Cerebus Neural Signal Processor at 30 kHz sampling rate. Automatic spike detection and spike sorting were performed on the electrophysiological signals recorded from each channel in each session using Spyking Circus.[68] This yielded the spike timestamps of single neurons during task trials at 1 kHz sampling rate.

We were particularly interested in examining whether LPFC-p inactivation had an effect on WM and attentional signals in visual and posterior parietal neurons (areas MT, MST and LIP). We therefore aimed at recording from sufficient neurons in these areas whose activity was modulated by LPFC-p inactivation. To this aim, we preferentially sampled recording locations that were the same as or

adjacent to those where we found modulated neurons in previous recording sessions. In left and right LPFC-p, we sampled recording locations relatively homogeneously within the region of opsin expression without regards to where modulation was observed in previous recording sessions.

In each area, we targeted neurons with motion direction selectivity during at least one of the task periods (cue, delay or test). Probe recordings with no direction-selective neurons were excluded from analysis, and the recording location was excluded from subsequent recording sessions. Recording locations were selected to be more proximal to previous recording locations with direction selective neurons and more distal from any locations without these neurons.

Optogenetic stimulation

Immediately before each recording session, we examined opsin expression by shining blue light (440–460 nm; NIGHTSEA TM) and visualizing/photographing green epifluorescence through a yellow filter (Figure 1D). Optogenetic stimulation was performed with two red lasers (635 nm) with adjustable power up to 4W (Shanghai Laser & Optics Century Co., Ltd., Shanghai). Each laser was coupled with a 2-m-long step index optical fiber with a ceramic ferrule end (400 μm core diameter, 2.5 mm optical density). Each fiber was firmly attached to a microdrive tower (parallel to it) fixed to the chamber so that the fiber end was located above the LPFC-p cortical surface on each hemisphere, pointing towards the center of the opsin expression region. During recording sessions, the LPFC-p chamber was sealed with two layers of black electrical tape that prevented any laser light from escaping the chamber. While no light was detectable from outside the chamber, an additional light-blocking black polyethylene film was tightly sealed around the monkey's implant margin to fully separate the implants from the area of visibility of the monkey.

The distance of the fiber end to the cortical surface ranged between 17 and 29 mm, and was chosen so the laser beam would cover the entire region of opsin expression. The laser beam diameter ranged between 8.5 and 9.5 mm in monkey Sh, and between 10 and 14.5 mm in monkey St. The laser power was adjusted so that the power density fell within the range of 30 to 42 mW/mm^2. In pilot experiments with a test monkey, this power range was found to successfully yield optogenetic inactivation of neurons across all cortical depths. Importantly, a previous study showed that cortical stimulation with a 635 nm laser at 100 mW/mm^2 (more than twice the power density used here) did not result in tissue heating greater than 1°C.[25]

In each recording session, the two lasers were simultaneously turned on in specific task periods in half of the trials (opto trials) and not in the remaining half (control trials). Opto and control trials were randomly interleaved. The lasers were automatically controlled by the behavioral task computer via TTL pulses. In a fraction of the sessions (delay-opto; 32 sessions in monkey Sh; 39 sessions in monkey St), the lasers were turned on for 2 s during the delay period, starting 300 ms after the sample stimulus offset, and ending 900 ms before the test onset. In the remaining sessions (test-opto; 23 sessions in monkey Sh; 43 sessions in monkey St), the lasers were turned on at the test onset, lasting for 2 s or until the monkey made a response. The laser stimulation regime was a single square pulse. Delay-opto and test-opto sessions were randomly interleaved, with sessions usually separated by at least a day in between.

Electrophysiological data analysis

All data analysis was performed using Matlab (Mathworks, Inc.). For each neuron, we calculated the firing rate over time across each trial in 50 ms bins. Trials were grouped by each combination of cue direction condition and optogenetic stimulation condition (control, delay-opto, test-opto). Using the Matlab function ROC,[69] we performed Receiver Operating Characteristics analysis to obtain the area under the ROC curve (auROC) comparing the distributions of firing rates across trials in pairs of conditions with opposite cue directions. This analysis was performed independently on the firing rates in the cue period (1000 to 1800 ms from trial onset), delay period (2100 to 4100 ms), and test period (5000 to 5900 ms), to obtain an estimate of sensory discriminability, WM discriminability and attentional discriminability, respectively (Figures 2C and 2E). auROC values between 0.5 and 0 were rectified to their corresponding values between 0.5 and 1 in order to quantify direction discriminability independently of direction preference. The same analysis was independently performed in control and opto trials. For the analyses of attentional discriminability and WM discriminability without optogenetic inactivation (Figure 2), neurons with significant direction discriminability (rectified auROC significantly higher than expected by chance) in at least one of the three periods (cue, delay or test) of control trials were considered direction selective and were included for subsequent analyses. Neurons with an average firing rate lower than 2 spikes/s or with less than 10 trials per condition were excluded. In test-opto sessions, the resulting neuron sample sizes for each brain area were 557 in LPFC-p, 395 in MT, 690 in MST, 289 in LIP. In delay-opto sessions, the resulting neuron sample sizes for each brain area were 572 in LPFC-p, 489 in MT, 1048 in MST, 229 in LIP. For each neuron, auROC values were also calculated after randomly shuffling the direction condition labels between trials. This provided an estimate of the mean (± standard error) auROC across neurons in each area expected by chance (Figure 2C).

Because our main aim was to measure the effects of optogenetic LPFC-p inactivation on task performance and on each neuron's WM coding and feature attentional modulation strength, our analyses included correct and error trials (target responses, early responses, distractor responses and no responses). As described previously, monkey Sh was trained to perform the task with 4 possible cue directions. For this monkey, ROC analysis in each task period was performed on each pair of opposite cue direction conditions. If one pair of directions showed significant auROC, this pair was chosen for subsequent analyses. If both direction pairs showed significant auROC, the pair yielding the highest discriminability (the most aligned to the neuron's direction preference axis) was selected for further analyses. From the selected pair of directions, the one for which the neuron showed the highest mean activity across trials was identified as the preferred direction. Chi-square tests for proportions were used to test for significant differences

between the proportion of WM & attention, WM-only, and attention-only neurons within each area, for significant differences in the proportion of WM & attention neurons between areas. For each of these groups of tests, significance was assessed after a Bonferroni correction for multiple comparisons. To test the relationship between WM and attentional discriminability (Figure 2E), we used Spearman's correlation. This test was more appropriate than Pearson's correlation given that some brain areas showed unequal variances across different auROC ranges. To determine whether each neuron showed an excitatory response to the cue, we tested whether the mean firing rate across trials was significantly higher during the cue period than the fixation period using a one-tailed unpaired t test. A similar comparison of mean firing rate during the delay vs. the fixation period was used to determine whether each neuron showed delay activity.

For each neuron with cue, delay, or test period direction discriminability in control or test-opto trials, we performed a two-way ANOVA with cue motion direction and optogenetic condition (test-opto vs. control) as factors, and test period firing rate as the dependent variable. Neurons with a significant overall main effect of optogenetic condition and/or a significant interaction effect were classified as showing significant test period optogenetic modulation of firing rates (Figures 4A–4D and 4I). The numbers of such neurons in each area were: 218 in LPFC-p, 211 in MT, 309 in MST, and 77 in LIP. These neurons were used to obtain the results in Figures 5B–5I and S6A–S6D. An equivalent procedure was used to classify neurons as showing significant delay period optogenetic modulation of delay period firing rates (Figures 4E–4H and 4J). The numbers of such neurons in each area were: 283 in LPFC-p, 291 in MT, 612 in MST, and 89 in LIP. These neurons were used to obtain the results in Figures 6B–6G and S6E–S6G. An equivalent procedure was used to determine whether neurons showed significant delay period optogenetic modulation of test period firing rates (Figures 4E–4H and 4K). It is important to note that in all the above analyses, we selected neurons by direction discriminability in both control and opto conditions to prevent any selection bias that could artificially favor higher auROC values in the control condition over the opto condition (i.e., "double-dipping").

In the population analyses used to produce the results shown in Figures 4E–4K, 5B–5E, 6B–6D, and S5A–S5H, the firing rate over time of each neuron in each condition was normalized by dividing by its mean firing rate across the entire time period of interest and across all conditions compared. Plots of mean firing rate over time (Figures 1E, 1F, 2A, 4A–4H, 5A–5E, 6A–6D, and S5A–S5H) were obtained by convolving the binned firing rates in each trial with a 200 ms kernel and then obtaining the mean and standard error of these traces across trials. This data was used to calculate auROC over time for each neuron and obtain the mean auROC and standard error across neurons over time (Figures 5F–5I and 6E–6G). For each neuron, the auROC expected by chance was obtained by repeating the same procedure after randomly permuting the cue direction condition labels between trials, independently in control and opto conditions. To test for inactivation-induced reductions in attentional or WM discriminability over time in each area, we compared the mean auROC values across neurons between opto and control conditions at all test or delay period time bins using one-tailed Wilcoxon rank sum tests. Significance was reached when a pair of consecutive time bins showed p values < 0.05. This criterion corrected for multiple comparisons. To obtain the latency of optogenetic modulation of firing rates for each neuron, we used a sliding 20-ms window by steps of 1 ms to find the earliest 20-ms window at which the mean firing rate across opto trials significantly deviated from control trials by an unpaired t test ($p < 0.05$), and at which significance persisted in the following 4 consecutive steps of 1 ms. For each neuron with significant test-opto modulation of firing rates, we computed an attention auROC modulation index measuring the percent change in attentional discriminability between control and test-opto conditions at each time bin during the test period. Similarly, for each neuron with significant delay-opto modulation of firing rates, we computed a WM auROC modulation index measuring the percent change in WM discriminability between control and delay-opto conditions at each time bin during the delay period. The following equation was used for both indices:

$$\text{auROC modulation index} = (\text{auROC}_{\text{opto}} - \text{auROC}_{\text{ctrl}}) \,/\, \text{auROC}_{\text{ctrl}}$$

For each brain area, we then calculated a frequency histogram showing the distribution of attention auROC modulation indices across neurons at each time bin during the test period (Figures S6A–S6D), and a frequency histogram showing the distribution of WM auROC modulation indices across neurons at each time bin (Figures S6E–S6G).

For the results in Figures 5J and 5K, we tested whether the percentage of neurons with significant attentional discriminability, and the mean attentional discriminability (auROC) across those neurons, were lower in test-opto trials than in control trials. Because control trials from both test-opto and delay-opto sessions were identical, we analyzed neuronal responses from both to increase neuronal sample sizes and improve the accuracy of our estimates. This was possible because these analyses were between-neurons and not within-neuron. A one-tailed Wilcoxon rank sum test was used to compare mean attentional discriminability in test-opto vs control (Figure 5J). For this test, the neuron sample sizes in the control condition were: 402 in LPFC-p, 210 in MT, 487 in MST, and 319 in LIP; the neuron sample sizes in the test-opto condition were: 221 in LPFC-p, 110 in MT, 230 in MST, and 193 in LIP.

An equivalent procedure was performed to test whether the percentage of neurons with significant WM discriminability and the mean WM discriminability (auROC) across those neurons were lower in delay-opto trials than in control trials (Figures 6H and 6I). For the Wilcoxon rank sum test (Figure 6H), the neuron sample sizes in the control condition were: 455 in LPFC-p, 592 in MST, and 268 in LIP; the neuron sample sizes in the delay-opto condition were: 237 in LPFC-p, 334 in MST, and 96 in LIP. An equivalent procedure was performed to test whether the percentage of neurons with significant attentional discriminability and the mean attentional discriminability (auROC) across those neurons were lower in delay-opto trials than in control trials (Figures 6K and 6L). For the Wilcoxon rank sum test (Figure 6K), the neuron sample sizes in the control condition were: 402 in LPFC-p, 210 in MT, 487 in MST, and

319 in LIP; the neuron sample sizes in the delay-opto condition were: 218 in LPFC-p, 122 in MT, 307 in MST, and 134 in LIP. For Figures S6I and S6J, a neuron showed a cue response or delay activity if its mean firing rate was significantly higher in the cue period or delay period than the fixation period across trials, respectively (paired t tests).

Population decoding

For the results in Figures S4 and S6J, we applied multivariate classification analysis using the Neural Decoding Toolbox in Matlab[70] to decode the cue direction from the firing rate patterns of the neuronal population during the delay period (directions in WM) and test period (attended directions). Decoding was performed in 400-ms bins at steps of 100 ms. We applied Z-scoring normalization feature preprocessing to each neuron's firing rates and excluded neurons with less than 15 trials per direction condition. We then ran a maximum correlation coefficient classifier with cross validation using 15 cross-validation splits. Direction decoding performance was obtained using the Receiver Operating Characteristics (ROC) curve method, combining all decision values over all cross-validation splits. This procedure was repeated over 30 resamples, and decoding performance was averaged across all resamples. For Figure S4, mean decoding performance (± standard error) for directions in WM and for attended directions was obtained by computing the mean performance (± standard error) across time bins during the delay (excluding the first 300 ms and the last 900 ms) and during the test period, respectively. For Figure S6J, decoding analysis was performed separately on control and delay-opto trials. To determine whether decoding performance was significantly lower in delay-opto than control trials in each time bin, we repeated the above analysis over 500 permutations, each time after control and delay-opto trials were combined and randomly split again into surrogate control and delay-opto conditions. At each time bin, the p value for the difference between decoding performance in control and delay-opto trials (control – opto) was calculated as the proportion of permutations for which the decoding performance difference was greater than the difference in the original data. Decoding performance was significantly lower in opto than control trials in time bins with a p value lower than 0.01 (accounting for multiple comparisons).

Spike waveform analyses

To classify neurons as putative excitatory (broad-spiking) or putative inhibitory (narrow-spiking) neurons, we performed standard spike waveform analyses.[71] Briefly, for each neuron, we calculated the width of the mean spike waveform (trough-to-peak time). The distribution of spike widths across all neurons was bimodal, and the trough between the two peaks served as boundary to classify neurons as putative excitatory (broad-spiking) neurons as putative inhibitory (narrow-spiking) neurons.

Neuron, Volume *112*

Supplemental information

Dissociable neuronal substrates of visual feature attention and working memory

Diego Mendoza-Halliday, Haoran Xu, Frederico A.C. Azevedo, and Robert Desimone

Supplemental Figures

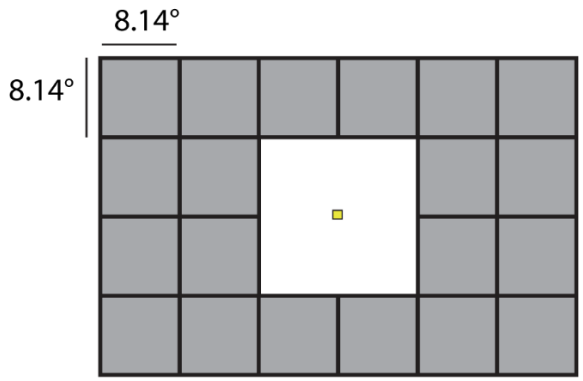

Figure S1. Alternative locations of target/distractor speed change patches across the visual display (Related to Figure 1A). In each trial, patch locations were chosen randomly among all locations (gray squares). Fixation point is yellow. Patch size is shown in visual degrees. Patch locations overlapping with the fixation point or fixation window were excluded.

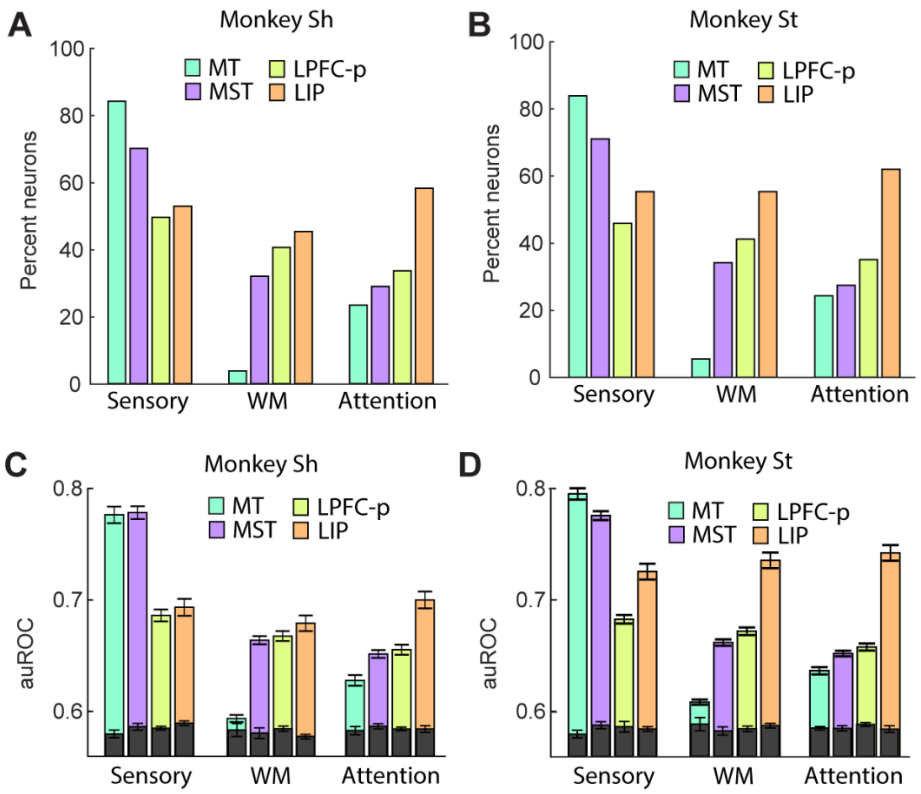

Figure S2. Effects of WM and attention shown separately for the two monkeys (Related to Figure 2).

(A,B) Percentage of neurons with significant sensory, WM, and attentional discriminability in each brain area, shown separately for the two monkeys. (C,D) Mean (± standard error) sensory, WM, and attentional discriminability across all neurons in each brain area, shown separately for the two monkeys. Gray bars, mean (± standard error) auROC expected by chance.

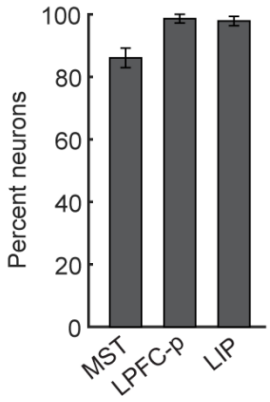

Figure S3. Relationship of motion direction preference during WM and attention (Related to Figure 2).
Percentage of WM & attention neurons in each area for which WM coding and attentional modulation showed the same motion direction preference. MT was excluded due to the low number of WM & attention neurons.

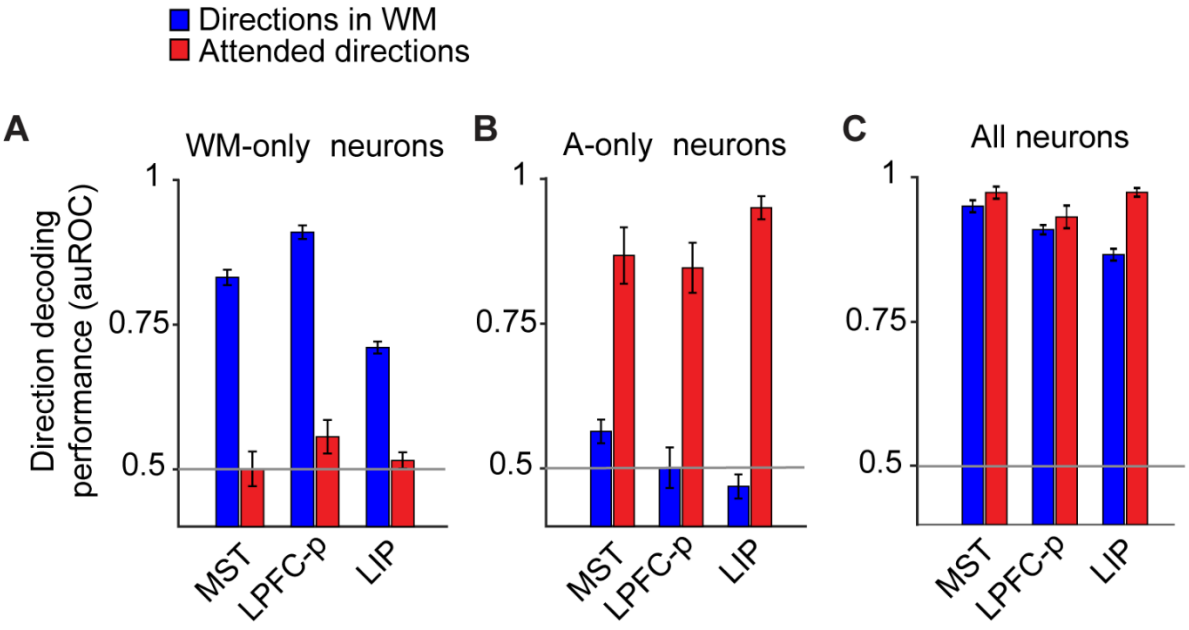

Figure S4. Population decoding of motion directions in WM and attended directions (Related to Figure 2).
Mean decoding performance (measured as auROC) of cue direction across time bins during the delay period (blue, directions in WM) or test period (red, attended directions) for a multivariate classifier trained on the population activity patterns of WM-only neurons (A), attention-only neurons (B), and all neurons, including WM-only, attention-only, and WM & attention (C).

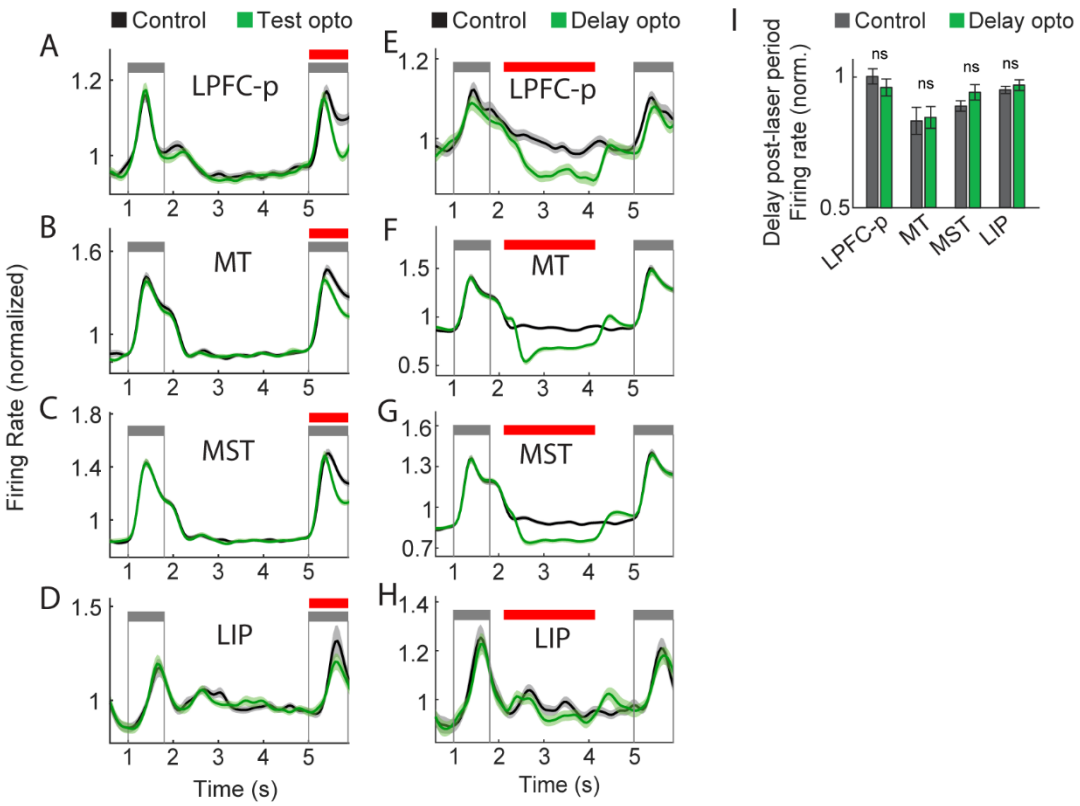

Figure S5. Effects of test and delay period optogenetic prefrontal inactivation on firing rates across all neurons in each area, and delay period inactivation effects on post-stimulation interval mean firing rates (Related to Figure 4).

(A-H) Mean normalized firing rate (± standard error) over time in control and opto trials across all neurons in LPFC-p, MT, MST, and LIP during sessions with optogenetic stimulation during the test period (A-D) or delay period (E-H). Each neuron's firing rate was normalized by its mean firing rate across all trial periods and conditions. Firing rate decreases are visible in the mean across all neurons, although less pronounced that in the mean across significantly modulated neurons (Fig. 4). (I) Mean normalized firing rate (± standard error) during the post-stimulation interval of the delay period (from 200 ms after laser offset until the delay end) in control and opto trials across neurons with significant modulation during the optogenetic stimulation period. ns, not significant ($P \geq 0.05$).

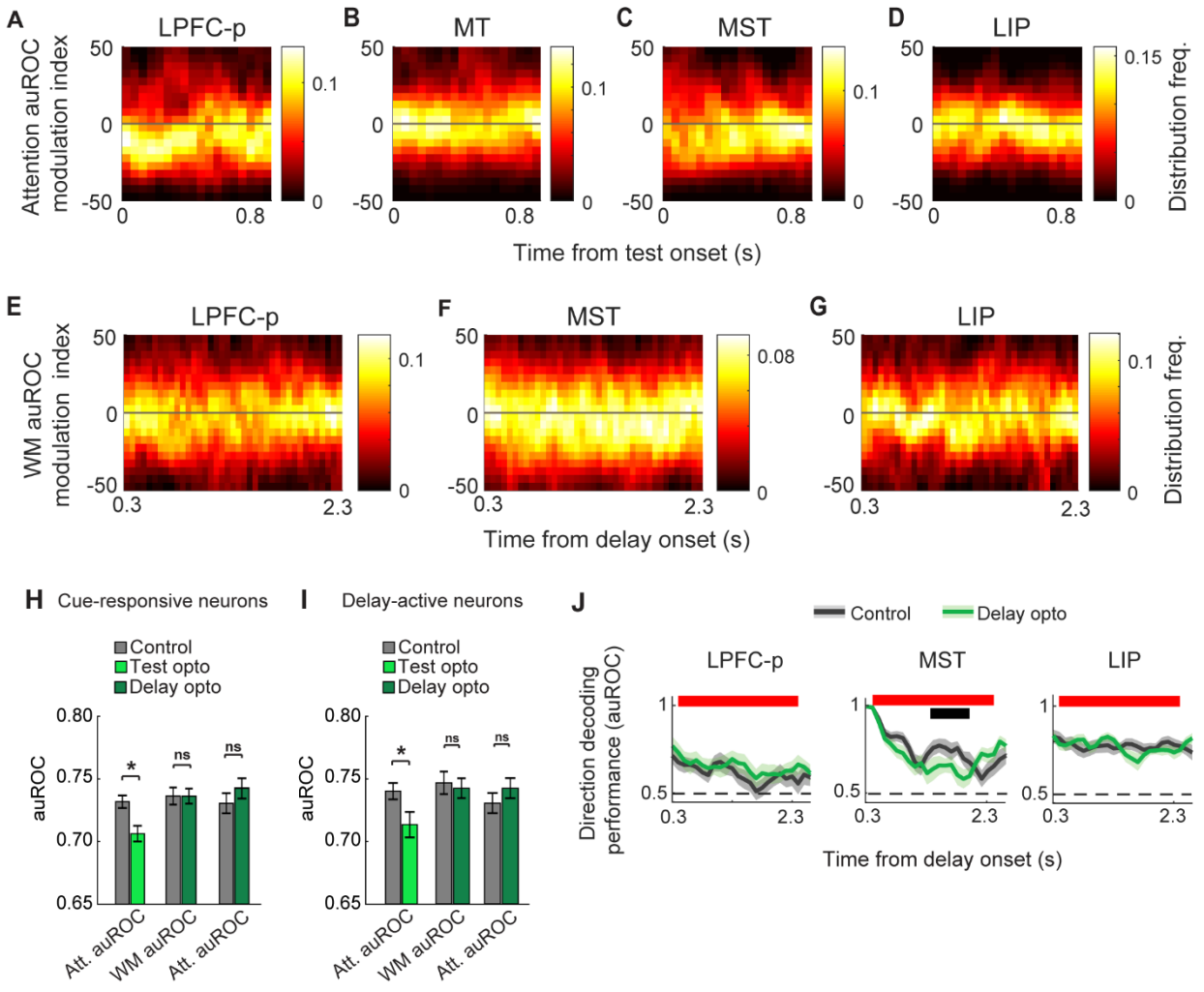

Figure S6. Effects of optogenetic prefrontal inactivation on WM and attention discriminability and on population decoding of memorized motion directions (Related to Figures 5,6).

(A-D) Distribution of attention auROC modulation indices across neurons in each brain area with significant optogenetic firing rate modulation over time during the test period. (E-G) Distribution of WM auROC modulation index across neurons in each brain area with significant optogenetic firing rate modulation over time during the delay period. (H,I) Mean attention or WM auROC (± standard error) across cue-responsive (H) or delay-active (I) LPFC-p neurons with significant discriminability in control and test-opto or delay-opto trials. *, $P < 0.05$. ns, not significant. (J) Motion direction decoding performance (mean auROC ± standard deviation across 30 resamples) during the delay period in control and opto trials, for the neuron populations in LPFC-p, MST, and LIP. Red segment, optogenetic stimulation period; black segments, time bins with significant decoding performance difference between control and opto trials; dotted lines, decoding performance chance value.

Supplemental Tables

Task period	Cue (Sensory)	+	+				+	+
	Delay (WM)		+	+	+			+
	Test (Attention)				+	+	+	+
Area	MT	674	27	12	2	136	82	5
	MST	890	188	267	62	216	135	107
	LPFC-p	403	94	335	58	278	69	34
	LIP	98	32	95	36	129	50	130

Table S1. For each area: Number of direction-selective neurons with significant direction discriminability in each combination of task periods (+). These values are depicted in the Venn diagrams of Figure 2D.